Journal of Pharmaceutical Sciences 112 (2023) 2463–2482

Contents lists available at ScienceDirect

Journal of Pharmaceutical Sciences

journal homepage: www.jpharmsci.org

Pharmaceutics, Drug Delivery and Pharmaceutical Technology

Applying Material Science Principles to Chemical Stability: Modelling Solid State Autoxidation in Mifepristone Containing Different Degrees of Crystal Disorder

Jayant Iyer[a], Lucy M. Morgan[b], Pamela Harrison[c], Adrian Davis[b], Andrew Ray[d], Stefan Mitsche[e], Ferdinand Hofer[e], Isha Saraf[a], Amrit Paudel[a,f,*]

[a] Research Center Pharmaceutical Engineering GmbH (RCPE), Graz 8010, Austria
[b] Pfizer Worldwide Research, Development and Medical, Sandwich, Kent, CT13 9NJ, UK
[c] Oral Product Development, Pharmaceutical Technology and Development, operations, AstraZeneca, Macclesfield SK10 2NA, UK
[d] New Modalities & Parenteral Development, Pharmaceutical Technology & Development, Operations, AstraZeneca, Macclesfield SK10 2NA, UK
[e] FELMI ZFE-Austrian Center for Electron Microscopy and Nanoanalysis Graz University of Technology, Graz 8010, Austria
[f] Graz University of Technology, Institute of Process and Particle Engineering, Graz 8010, Austria

ARTICLE INFO

Article history:
Received 7 January 2023
Revised 27 March 2023
Accepted 28 March 2023
Available online 7 April 2023

Keywords:
Amorphous
Autoxidation
Crystal disorder
Mifepristone
Partially crystalline
Solid-state degradation

ABSTRACT

Ball-milling and harsh manufacturing processes often generate crystal disorder which have practical implications on the physical and chemical stabilities of solid drugs during subsequent storage, transport, and handling. The impact of the physical state of solid drugs, containing different degrees/levels of crystal disorder, on their autoxidative stability under storage has not been widely investigated. This study investigates the impact of differing degrees of crystal disorder on the autoxidation of Mifepristone (MFP) to develop a predictive (semi-empirical) stability model. Crystalline MFP was subjected to different durations of ambient ball milling, and the resulting disorder/ amorphous content was quantified using a partial least square (PLS) regression model based on Raman spectroscopy data. Samples of MFP milled to generate varying levels of disorder were subjected to a range of (accelerated) stability conditions, and periodically sampled to examine their recrystallization and degradation extents. Crystallinity was monitored by Raman spectroscopy, and the degradation was evaluated by liquid chromatography. The analyses of milled samples demonstrated a competition between recrystallization and degradation via autoxidation of MFP, to different extents depending on stability conditions/exposure time. The degradation kinetics were analyzed by accounting for the preceding amorphous content, and fitted with a diffusion model. An extended Arrhenius equation was used to predict the degradation of stored samples under long-term (25°C/60% RH) and accelerated (40°C/75% RH, 50°C/75% RH) stability conditions. This study highlights the utility of such a predictive stability model for identifying the autoxidative instability in non-crystalline/partially crystalline MFP, owing to the degradation of the amorphous phases. This study is particularly useful for identifying drug-product instability by leveraging the concept of material sciences.

Introduction

The stability of pharmaceutical products is considered a critical attribute[1,2] as it ensures the safety and efficacy of the therapeutics throughout the intended shelf-life. During the pharmaceutical development, rigorous stability testing is performed for (1) developing robust formulation design, (2) selecting appropriate manufacturing processes, (3) identifying appropriate packaging (container-closure), and (4) setting the desired shelf-life specification.[3] Instability within drug products can cause significant reduction in the potency of administered dose, loss of product performance (*e.g.* dissolution failure of solid product), formation of (geno-)toxic degradants, possibility of adverse events or side-effects, shortened shelf-life that can cause supply chain issues, batch variations and/ recalls, etc.[4] Among the reported mechanisms of instabilities, oxidation in pharmaceuticals has been proven as a challenging risk owing to multiple factors.[5] Firstly, oxygen is ubiquitous in the environment, and reducing or eliminating its interaction with the product is not straightforward. Secondly, the predicting/ identifying oxidation risk is often a

* Corresponding author at: Address: Inffeldgasse 13, 8010, Graz, Austria.
E-mail address: amrit.paudel@rcpe.at (A. Paudel).

https://doi.org/10.1016/j.xphs.2023.03.020

formidable task due to complicated reaction mechanisms (e.g. involving free radicals); the kinetics of degradation may have an induction period, where hardly any degradation could be detected.[6] Additionally, there is an open question about mitigation strategies (rational selection of an antioxidant) and their efficacy.[7] Routine stability studies of pharmaceuticals are time-consuming, and any late-stage stability issues are often disappointing. Hence, the pharmaceutical industry has been striving to adopt alternative approaches that use short-term accelerated stability models to predict, and assess the risk to long-term storage stability.[4,8] Research in this area has also shown promise in enabling quality by design paradigm in the context of pharmaceutical regulatory acceptance.[9,10]

Milling is widely considered as an operation of choice for particle size reduction, homogenization of a blend, and to facilitate mixing.[11] Uniformity and fine particle size of a drug powder prepared by milling generally facilitates processability, enhances dissolution of poorly water-soluble drugs, and improves aerosolization of inhaled drugs.[12,13] On one hand, changes in the hygroscopicity, surface-texture, porosity, density, surface-free energy, and surface-area is commonly observed at the particle and powder level upon milling.[14] On the other hand, several reports have highlighted that milling can generate crystal defects by amorphization.[15–17] The quantity and physical state of such crystal defects may have severe implications on the downstream drug stability,[18] flowability,[19] and therefore, on batch-to-batch uniformity. Owing to the metastable nature of the defect sites of crystal lattice generated upon milling, they are the *hot spots* triggering physical and chemical transformations.[20] Modhave et al. reported on the autoxidation of simvastatin owing to the generation of a metastable amorphous state during milling.[21] Disordered crystals of an antifungal drug were shown to autoxidize in the amorphous state.[22] Similarly, autoxidation in the solid-state has been exemplified as a key instability for representative drugs, namely, Olanzapine,[23] Tetrazepam,[24] and Sirolimus.[25] A steroidal sulfatase inhibitor was shown to degrade by multiple mechanisms when milled.[26] Schenk et al. reported on the shear sensitivity of a drug which led to its oxidation upon common processing. They also point out that amorphization resulting from shear could be mitigated by coprocessing the drug.[27] Otsuka et al. have reported chemical degradation in Cephalothin by the influence of compression or grinding.[28,29] Also, drug degradation in the solid state was reported to increase as a function of amorphous content and the storage conditions.[30,31] Several reports on milling-induced physical instabilities such as polymorphic conversion, recrystallization or desolvation are known to occur upon milling.[31-34] As milling generates a diverse range of (metastable) amorphous fraction, a systematic study of evolution of solid-state properties during storage is important. Various studies have indicated the impact of annealing on solid particles post milling.[36,37] At the molecular level the annealing/ageing process is often accompanied by a reduction in the molecular mobility and re-crystallization of disordered solid states. In the case of stable (rigid) amorphous solid-fraction, where the recrystallization rate is slower, the residual amorphous phase can undergo chemical degradation. Although disordered phase is known to be responsible for the chemical degradation of pharmaceutical solids, the evolution and consequence of such crystal defects upon storage is seldom reported.

The kinetics and extent of an amorphous drug degradation depends on the rates of recrystallization under respective storage conditions. Ideally, the high-energy solid states generated during milling would experience a competition of driving forces between degradation and recrystallization in the course of subsequent storage. Several reports have aimed to correlate and compare the rates of recrystallization and degradation to the molecular mobility of the amorphous solid.[38,39] Previous research has also indicated diverse approaches to modelling the degradation of pharmaceutical solids based on application of a modified Arrhenius equation. For example, Tamura et al.[40] have proposed a polynomial model, where the degradation of Aspirin formulations depended on the level of magnesium stearate. Patterson et al.[41] have used a modified Arrhenius model by incorporating a term for succinic acid content to predict the drug degradation in a spray dried amorphous polymeric dispersion. Klemen et al.[42] has proposed a non-linear kinetic model to evaluate the pressure sensitivity of Candesartan cilexetil. Prediction of individual degradation products concentration in Saxagliptin coated tablets was achieved by considering formulation factors.[43] The prime utility of such models is to provide mechanistic insight into drug degradation (by incorporating manufacturing stress, formulation factors), and thereby generating accurate predictions of a drug's shelf-life in a short time.

Herein, we explore the impact of milling-induced crystal disorder on the autoxidation of Mifepristone (MFP) during accelerated stability storage conditions combining diverse temperatures and relative humidities (RH). The residual crystallinity of MFP samples during stability storage was quantified using Raman spectroscopy. By assuming the amorphous fraction as the main substrate for both re-crystallization and autoxidation, we analyzed the autoxidation kinetics accounting the amorphous content existing at preceding stability time point. Thereafter, a diffusion model was fitted to the experimental degradation kinetics. The obtained autoxidation rate constant allowed application of an extended Arrhenius model to predict the degradation of milled samples stored under long-term stability conditions. This is a novel attempt to model the degradation of disordered solids using a semi-empirical approach and considering the recrystallization phenomenon, as an incentive to apply solid material science. Simultaneously, we evaluated the implication of plasticization and ageing/annealing of disordered MFP solids on the reproducibility of degradation in multiple laboratories. Our work is useful for evaluating the impact of processing a crystalline as well as for amorphous pharmaceutical solids that undergo autoxidation upon storage by fostering the applicability of predictive stability models.

Experimental

Materials

Crystalline Mifepristone (MFP) was purchased from Quingao Dacon (China) (99.60% by assay). 2,2′-Azobisisobutyronitrile (AIBN) was purchased from Merck (Vienna, Austria). Weighing of solid powders was done using laboratory analytical balances. Ultrapure water was obtained from a TKA water purification unit. A laboratory oven from Binder® (Tuttlingen, Germany) was used to expose the samples under different stability storage conditions. HPLC grade acetonitrile (ACN) was obtained from VWR Chemicals (Dresden, Germany). Buffer ammonium formate (AF), and all other chemicals were of analytical reagent grade.

Method

Room Temperature Milling to Generate Amorphous Content

MFP was ball-milled at room temperature using a Retsch Cryo mill (Retsch GmbH, Germany) using a single stainless-steel ball of 2.0 cm diameter and 25 Hz milling frequency. Approximately, 3 g solid MFP was filled in a 50 mL milling jar and individual samples were separately ball-milled continuously for 5, 15, 30, 45, 60, 90, 120, and 180 min respectively, to generate different levels of amorphous content. In addition, separate samples were also milled for 1, 2, 3, and 10 min to investigate the initial amorphization kinetics. Subsequent to milling, the powder was scraped from the milling jar using a metallic spatula, and stored under nitrogen-purged amber glass vials to prevent oxidation. Entire sample collection step was performed inside an isolator glove box to prevent accidental dust exposure, and the collected solid was stored in a freezer at −20°C.

Differential Scanning Calorimetry

Differential scanning calorimetry (DSC) were carried out on samples using a DSC 204 F1 Phoenix (Netzsch, Germany) equipped with intra-cooler and an autosampler. Indium and Zinc were used for calibration of temperature and enthalpy. Approximately, 10–15 mg of sample was placed in an aluminum pan and covered with a pin-holed lid. The sample pans were heated at a controlled 5°C min^{-1} heating ramp from 0°C to 250°C under N_2 flow. All milled samples were analyzed immediately after milling using this single heating run method.

To evaluate the degree of plasticization and change in T_g in the samples exposed in stability conditions, modulated DSC was performed. Samples were heated in hermetically sealed pans from 0°C to 250°C under N_2 flow at a heating rate of 5°C min^{-1}. A modulation amplitude of ±0.541°C, and a 40 s period was applied, and the T_g was examined in the reversing mode.

Scanning Electron Microscopy (SEM)

In order to visualize the effects of milling, the surface morphology of the 5, 15, 180 min ball-milled and cryo quench cooled MFP samples was examined with a scanning electron microscope (SEM). To avoid charging during SEM imaging, all samples were coated with an AuPd layer (a few nanometers). Images were acquired on a Zeiss Ultra 55 field emission gun scanning electron microscope at an accelerating voltage of 5 kV and a beam current of 0.19 nA. The electron detector used was a Everhart-Thornley detector, in which topographic contrasts are mainly visible.

Raman Spectroscopy

Raman analysis of samples was performed on Perkin Elmer Raman station 400F (Perkin Elmer, Germany). A small quantity of sample was placed in the centre of the brass sample holder. A mapping method was used at 12 different points to cover the height and width of slide matrix with spectral acquisition at 10 scans per point. Laser intensity was kept at 80%, and an exposure time of 1 s was applied. Finally, the scans were co-added to yield an average spectrum. The acquired scans ranged from wavenumbers 200–2500 cm^{-1}. The interpretation of spectra was performed by using SpectraGryph® software version 1.2.15 (Oberstdorf, Germany).

To quantify the crystallinity of ball milled (BM) MFP samples, a calibration curve was developed using 180 min BM (amorphous) MFP and crystalline MFP. The two solids were physically mixed to generate different degree of crystalline content ranging from 10%–90% crystallinity in increments of 10% crystallinity along with controls (0% and 100% crystallinity) and spectra were acquired using the method as described above. Triplicate samples at each crystallinity interval (n = 3) were generated, out of which the first two sets were used as calibration samples, while the third set was used for validation. All spectral pre-processing was done in SIMCA (version 17, Umetrics, Sweden); the range of 1540 −1700 cm^{-1} was selected, and the variables were mean centered. The spectral pre-processing steps consisted of (1) peak height normalization (2) standard normal variate (SNV) normalization and (3) asymmetric least square smoothing (AsLS) correction using a smoothing factor of 10000, and an asymmetry factor of 0.001. The performance of the developed model was evaluated by using correlation coefficient (R^2), test set validation coefficient (Q^2), root mean square error of estimation (RMSEE) and root mean square error of prediction (RMSEP).

Wide Angle X-ray Scattering and Variable Temperature Scans

WAXS measurements were acquired using a Hecus® S3-MICRO (Bruker, Germany) instrument operating at 30 kV/0.4 mA to generate X-ray from a Cu Kα source. The system encompasses S3-MICRO SWAXS (Hecus®), and a point-focusing detector (2Hecus PSD-50; 54 μm/channel) that enables recording of X-ray scattering in the range of 17–27° 2θ (WAXS). The powder samples were placed in sealed quartz capillary and measured in transmission mode with rotating capillary setup. To monitor the polymorphic change in MFP samples at different temperatures a variable temperature scan was performed at different temperatures namely, 25°C, 70°C, 110°C, 140°C, 160°C, 170°C and 190°C. A hold time of 1200 s was used at each temperature to stabilize the sample, and a WAXS scan was acquired after every 600 s increment. The purpose of variable temperature experiment was to interpret the different thermal events observed during the DSC heating run of ball-milled MFP samples.

Powder X-ray Diffraction (PXRD)

Powder X-ray diffraction (PXRD) was used to determine the degree of crystallinity in the milled samples. Samples were analyzed by using a Siemens D5005 X-ray diffractometer (Munich, Germany) configured with Bragg-Brentano geometry that uses Cu Kα (1.5418 Å). 40 kV voltage and 40 mA current were used and scans were performed from 7°–30° 2θ. The selected step size was 0.04°, and the counting time was 2 s/step. The resulting data was plotted as an overlay in Origin software.

Dynamic Vapor Sorption (DVS)

The moisture sorption behavior of amorphous MFP solids was investigated with DVS (Advantage, Surface Measurement Systems, Alperton, U.K.). The temperature was set to 25 ± 0.5°C and water was used as the probe vapor. Appropriate partial pressures (P/P_0) were controlled by mixing the water vapor with dry nitrogen gas with mass flow controllers. The degree of weight change was measured by a highly sensitive microbalance. Approximately, 35–45 mg of powder was weighed and subjected to 0%–90%–0% RH in 10 %RH steps for allowing sorption and desorption isotherms. A 4 h equilibration window was provided at each of the RH interval. The system was considered as equilibrated if the rate change in mass was less than 0.002% min^{-1}. Samples were pre-treated at 0 %RH to ensure they were dry.

Accelerated Stability Evaluation

The impact of degradation and recrystallization was assessed by subjecting the samples to different accelerated storage conditions namely, 40°C/75 %RH, 40°C/10 %RH, 50°C/10 %RH, 50°C/75 %RH, 70°C/10 %RH and 70°C/75 %RH in a stability chamber (WTC Binder, Germany). In total, five different types of solid samples were selected, namely, the unmilled crystalline MFP, 5- and 15 min BM MFP (partially crystalline), 180 min BM MFP and cryo-quench cooled (QC) MFP (amorphous). In each case, approximately 10–15 mg sample was weighed in amber-colored high-performance liquid chromatography (HPLC) vials and stored openly in desiccators equilibrated with the respective humidity. Saturated salt solution of sodium chloride (NaCl) was used to maintain 75 %RH, while Lithium chloride (LiCl) was used to maintain 10 %RH. Samples for long-term stability evaluation were stored in a stability chamber preset to 25°C/60 %RH. Approximate time elapsed between the day on which the milled samples were prepared and the day on which the samples were loaded under stability conditions was around 120 d. The samples were stored (in an amber glass vial, nitrogen purged, with parafilm wrapped) in a freezer at −20°C. Samples were pulled out from stability chamber on respective days as shown in Table 1, and analyzed for crystallinity (using Raman spectroscopy) and chemical degradation (using UPLC). Moisture uptake in the samples stored under different conditions was measured by gravimetric technique. Pre-weighed samples were exposed to the mentioned stability conditions and were re-weighed at the end of exposure. The degree of moisture uptake was calculated from Eq. 1:

Table 1
General stability study protocol utilized to evaluate competition between recrystallization and degradation kinetics of selected samples: unmilled MFP, 5 min ball-milled (BM) MFP, 15 min BM MFP, 180 min BM MFP and cryo QC MFP.

Temperature (°C) ± 1°C	Relative humidity (%RH) ± 5%	Duration (days-d) and samples (n = 3)							
		0 d	3 d	8 d	15 d	30 d	60 d	90 d	180 d
Initial		2	-	-	-	-	-	-	-
40	75	-	3	3	3	3	3	3	3
50	75	-	3	3	3	3	3	3	-
40	10	-	3	3	3	3	-	3	3
50	10	-	3	3	3	3	3	3	-
70	10	-	3	3	3	3	-	3	-
70	75	-	3	3	3	3	-	3	-
25	60	-	-	-	3	3	3	3	3*

* samples were withdrawn at the end of 155 d

$$\%\ \textit{Moisture gain} = \frac{\text{Vial weight (after stability exposure)} - \text{initial weight of vial}}{\text{initial weight of vial}} * 100 \quad (1)$$

Replication of Experiments and Stability Evaluation at Multiple Sites

Additional experiments were replicated partly at Pfizer U.K. Ltd., using the protocol mentioned in Table 2. Supplied (unmilled) MFP was milled using the protocol specified in section "*Room Temperature Milling to Generate Amorphous Content*", using a Retsch MM400 mixer mill (Retsch GmbH, Germany). Multiple lower milling timepoints were selected here: 1, 3, 5, and 15 min. A PLS-(Raman) calibration model for quantifying the crystallinity of milled samples was constructed using the data spectra from Bruker FT-Raman RAM II (Kent, U.K.). Powder samples were loaded into short NMR tubes which rotated in the beam while also moving vertically, tracing a helix like pattern over the sample. The laser power was set to 500 mWh, collecting and averaging over 128 scans. The scans ranged from wavenumbers 200–2500 cm^{-1}, and OPUS 8.1 software was used to acquire the spectra. An average of 3 calibration sets was used for generating a calibration model. Another individual set was used for validation. Spectral range and pretreatments used in the model were kept the same as mentioned in section "*Raman Spectroscopy*".

Samples for accelerated stability studies were prepared individually for each condition and timepoint, in separate 4-dram vials. The dram vials were covered with a membrane (tissue) and placed inside the relevant stability pot with the relevant humidity capsules which were open and covered with a membrane (filter paper) then sealed to be placed in the oven. Samples were stored at −20°C under N_2 for approximately 15 d between milling and staging to stability studies.

The experiments aimed to evaluate the competition between recrystallization and degradation were also performed at AstraZeneca Inc by using the protocol as mentioned in Table 3. Multiple samples were generated by milling MFP for 2-, 3, 5, 10, 15, 30, 90, and 180 min at RCPE which were then supplied to AstraZeneca. Samples were stored at 5°C in a refrigerator for approximately 180 d between milling and loading under stability conditions. Samples for evaluating degradation were stored and analyzed via the automated stability system, RPD Tool® (Accroma®, Muttenz, Switzerland). Samples were placed into bespoke vials alongside a saturated salt solution reservoir to control humidity and stored in racks at the desired temperature. At each of the time point, the system automatically removed the sample from storage, prepared the analyte solution and injected in the UPLC system.

Samples for Raman analysis were stored within vials and placed in jars which were stored in ovens at the relevant temperatures. Humidity for all samples was controlled using saturated salt solutions, either NaCl for maintaining approximately 75 %RH, and LiCl for 10 %RH. A method was developed for Raman analysis on the DXR3 Smart Raman (Thermo, US) using a bulk sampling method by placing at least a 1 cm depth of sample into a clear glass vial. A 785 nm laser, 50 μm pinhole aperture, and 30 mW laser power was used with the universal platform accessory. The method used 30 s x 10 sample exposures, beam expander of 3.0 mm and a focus of 200. A weight corrected PLS calibration model same as that mentioned in section "*Raman Spectroscopy*" was generated to quantify the crystallinity of the samples at each stability pull.

Ultra-Performance Liquid Chromatography (UPLC)

Degradation of samples was analyzed using Waters Acquity UPLC (Milford, USA) instrument. An InfinityLab Poroshell ec-C8 column (Agilent technologies, Vienna, Austria) (100mm*3 mm *i.d.*; particle size 2.7 μm) was used with a column temperature of 30°C. The eluent was analyzed with an equipped photo-diode array detector at 305 nm wavelength. A gradient program at flow rate of 0.35 mL/min employing 10 mM ammonium formate (pH 3.70) as buffer (A), and acetonitrile (ACN) as the organic modifier (B) were used. From 0 to 1 min, the composition of B was kept constant *i.e.* at 20%. From 1 to

Table 2
Stability testing protocol for experiments conducted at Pfizer U.K. Ltd. to evaluate the competition between recrystallization and degradation kinetics of selected samples: unmilled MFP, 1 min BM MFP, 3 min BM MFP, 5 min BM MFP and 15 min BM MFP.

Temperature (°C) ± 1°C	Relative humidity (%RH) ±5%	Duration (days-d) and samples (n = 1)				
		0 d	7 d	14 d	28 d	42 d
Initial		√	-	-	-	-
40	75	-	√	√	√	√
50	45	-	√	√	√	√
50	75	-	√	√	√	√

-: no sampling, √: sampling (n = 1)

Table 3
Stability testing protocol selected by AstraZeneca inc. to evaluate the competition between recrystallization and degradation kinetics of selected samples: 2, 3, 5, 10, 15, 30, 90, 180 min BM MFP.

Temperature (°C) ± 1°C	Relative humidity (%RH) ± 5%	Duration (days-d) and samples (n = 1)					
		0 d	7 d	14 d	21 d	28 d	56 d
Initial		RU	-	-	-	-	-
40	75	-	RU	U	RU	RU	U
40	10	-	RU	U	RU	RU	U
70	75	-	RU	U	RU	RU	U
70	10	-	RU	U	RU	RU	U

R = Raman analysis, U = UPLC analysis.

6 min, the composition of B was increased from 20% to 70% and maintained at 70% until 10 min. From 10 to 11 min, the composition of B was increased from 70% to 90% and held at 90% until 12 min. At 12.01 min, the composition of B was reduced to 20% until the end of run i.e. 15 min. A combination of MeOH:milli-Q water (70:30) was used as a diluent to dissolve the samples. The sample concentration was kept at 500 μg/mL and 0.5 μL was injected.

Quantification was performed by integrating the area under the peak of drug (AUP) and degradants thereby, enabling calculation of the relative area% of drug using Empower-3® software as shown in Eq. 2. The value 99.60 was calculated as per the label claim/purity of the purchased drug, considering the remaining (0.40%) to be from impurities.

$$\%AUP\ of\ drug = 99.60 - (\%AUP\ of\ DPs) \quad (2)$$

The degradation of sample during accelerated stability storage was determined using Eq. 3 (based on reduction in the %AUP of drug's peak at time 0 min *i.e.*, soon after milling).

$$\%degradation = (\%AUP\ of\ drug - \%AUP\ drug\ under\ stability\ conditions) \quad (3)$$

Forced Autoxidation in Solution and Solid States

In solution state, AIBN (azo radical initiator) in 5–20 mol% of drug concentration was used as the stressing agent to induce autoxidation.[44] The concentration of drug stock solution was kept 1000 μg mL^{-1} in MeOH:water 70:30, and half of the solution was mixed with equal volumes of AIBN solution (20 mM stock was prepared in MeOH). The final reaction mixture contained 500 μg mL^{-1} drug and 10 mM AIBN as the stressor. The reaction was carried out by keeping two replicate samples in amber volumetric flasks and placing in the oven at 50°C. Additionally, a drug solution devoid of AIBN and another AIBN solution devoid of the drug were placed, as controls, in the oven at 50°C. The solution stress test provided the feasibility of autoxidation, and enabled the development of a stability-indicating method.

Forced autoxidation in the solid state was conducted by employing a high temperature oxygen-pressurized device called as RapidOxy® (Anton Paar GmbH, Austria). Approximately, 10 mg of cryo QC MFP was placed in a DSC pan (n = 3) at 100°C, and exposed at 700 kPa for 2 d. In parallel, control samples were kept by exposing the cryo QC MFP samples under nitrogen pressures in the RapidOxy® by keeping the same temperature and exposure times.

LC-High Resolution Mass Spectrometry (LC-HRMS) and Tandem MS/MS

To characterize the formed degradants in the solid and solution states, LC-HRMS and MS^n studies were performed. The high resolution and MS/MS data was acquired on a ThermoFisher Orbirap Fusion Tribrid mass spectrometer interfaced to a ThermoFisher Vanquish UPLC (Macclesfield, U.K.). All data was acquired in a positive ion mode using heated electrospray ionization (HESI) source. The MS conditions were: capillary voltage 3500 V, vaporizer temperature 350°C, ion transfer tube temperature 325°C, sheath gas flow 50 arbitrary units, auxiliary gas flow 10 arbitrary units and sweep gas 1 arbitrary units. The MS/MS was performed in collision induced dissociation mode with a collision energy of 40%.

Kinetic Modeling

One of the prime objectives was to develop a semi-empirical model predicting the degradation rates under long-term conditions of disordered MFP. To the best of our knowledge, such a model accounting for the presence of disorder (or amorphous content) and the recrystallization phenomenon has not been discussed before. Although existing methods based on extended Arrhenius models consider the impact of relative humidity, there are seldom cases where such model is applied to the partially crystalline and amorphous samples undergoing competitive degradation and amorphous form crystallization.[45] It is also postulated in such cases that the preceding amorphous fraction accounts for the extent of degradation occurring in the successive time point, hence, dictating the overall degradation kinetics. Here, the amorphous fraction was calculated using the crystallinity values obtained from the Raman PLS-model (as described in the section "*Raman Spectroscopy*" applying Eq. 4 and Eq. 5.

As the unmilled standard MFP was not polymorphic phase pure, an adjustment on the Raman data was made to calculate the actual crystallinity values by accounting the effect of polymorphic conversion in the stability samples. For each time point, the difference between 100% crystallinity and the predicted crystallinity was added to all samples at that timepoint to remove the effect of the phase change from the effect of recrystallization of the amorphous fraction in the sample.

For each time point:

$$Corrected\ crystallinity = C_s + (100 - C_{std}) \quad (4)$$

Where C_s is the crystallinity of the sample and C_{std} is the crystallinity of the standard (unmilled).

$$Amorphous\ fraction\ (f_{am}) = \frac{100 - \%Crystallinity}{100} \ldots \quad (5)$$

For modeling the degradation of disordered solids (assuming that the crystalline phase undergoes negligible degradation and recrystallization), the actual degradation was normalized to account for the presence of preceding amorphous content by using Eq. 6.

$$Effective\ degradation\ (\%Dn) = (f_{am}) * actual\ degradation \quad (6)$$

It is considered here that the effective degradation values account for the presence of recrystallization occurring over the time (i.e., the amorphous fraction would decrease over time).

Next, the kinetics plot was fitted by using a diffusion model as shown in Eq. 7 with Origin Pro 2021 software (Northampton, Massachusetts, USA). Preliminary examination of the goodness of fit of the experimental degradation kinetics data to different solid state degradation models was performed, as proposed previously,[46,47] where the diffusion model was found to provide the best fit (data shown in supplement

Fig. S8) to the data. Moreover, a diffusion model was selected because the phenomenon like autoxidation would depend on the diffusion of oxygen, hence, oxygen diffusion is the rate-limiting step.

$$\textit{Effective degradation } \%Dn = k * \sqrt{t} \quad (7)$$

Here, k is the degradation rate constant (d^{-1}) and t is the exposure time in d. The kinetics plot was limited to 30 d for most of the samples, analogous to the commonly used iso-conversion approach.

The natural logarithms of the obtained degradation rates were determined using Microsoft Excel (Microsoft Office 2021, USA). The log transformed degradation rates (z-axis) were plotted against their respective storage temperatures (x-axis) and RH (y-axis) to generate a 3-dimensional plot. The data points were surface fitted using the extended Arrhenius eq. (Origin Pro 2021, OriginLab, USA), as shown in Eq. 8. The Levenberg-Marquardt algorithm was chosen to surface fit the reaction rates as it is widely used for non-linear least square fittings and provide a single fitting minimum. Higher temperature (70°C) conditions were not considered as they led to a significant propagation of error in extrapolation/prediction accuracies.

$$ln\ k = ln\ A - \frac{Ea}{RT} + B * RH \quad (8)$$

Here, $ln\ k$ is the natural log of degradation rate constant, $ln\ A$ is the pre-exponential factor, E_a is the activation energy (in kcal mol^{-1}), R is the gas constant (1.987 kcal mol^{-1}), $1000/T$ is the inverse of absolute temperature (in K^{-1}), B is the moisture sensitivity parameter and RH is the relative humidity (%). From the above obtained Arrhenius descriptors, rate predictions were determined at 25°C/60 %RH, and the calculated values were compared to the actual rates obtained under this condition. Comparison of the model predictions were made by eliminating the conditions one-by-one where recrystallization occurs (e.g., 40°C/75 %RH and 50°C/75%RH), and by including the actual degradation rate at 25°C/60 %RH.

Results

Characterization of Ball-Milled Mifepristone

Thermal Characterization of Disordered Phases

All the ball-milled samples indicated amorphization, as evidenced by the presence of a glass transition temperature (T_g) onset of 105.7°C in DSC thermograms (Fig. 1). A DSC thermogram of the sample milled for 5 min indicated an exotherm of non-isothermal crystallization having an onset temperature of 120°C. With an extension in milling time (from 15–90 min), there was an incremental shift of this onset of crystallization exotherm to higher temperatures. Also, the crystallization enthalpy (ΔH) increased from 17.88 J g^{-1} for 15 min milled sample to 53.05 J g^{-1} for 90 min milled sample. This event indicates that a higher proportion of amorphous solid is generated over increased milling time, and the amorphous phase resists to recrystallize as compared to the 5 min ball-milled sample. As the milling progresses from 30 min to 90 min, a second exotherm near the melting endotherm was also evident. The enthalpy of the second exotherm signal increases with increasing milling time, and becomes stable after 90 min, indicating that higher energy input does not lead to significant changes of this event.

Interestingly, at the end of 180 min milling there is an appearance of a single exotherm. The hypothesis here is that upon extended milling (180 min), the solid becomes excessively defective (vitreous) so that the resolution between surface and bulk recrystallization events during heating in DSC is potentially lost. Moreover, for the 180 min BM MFP, the enthalpies of exotherm and endotherm were almost equal, indicating a complete transformation of the solid to an amorphous state such that the amount recrystallizing during heating in DSC is the same as the amount melting. DSC analysis of an unmilled MFP (which contained a mixture of metastable and stable crystalline forms) sample showed the first melting endotherm (178.2°C) of the metastable crystal form followed by a small exotherm of crystallization to the stable form. Further, both the initial metastable form, and the converted stable form melt together at 192.8°C.[48] All the milled samples indicate the melting of stable form as evidenced by an endotherm having the same onset temperature of 192.8°C. The DSC scan of the cryo QC amorphous solid indicates a recrystallization exotherm followed by a melting event of the same (stable) crystalline form. The delayed crystallization event for the cryo QC sample could be due to its lower surface to volume, as compared to the milled counterparts. Although the ball-milled MFP samples were in glassy state (with the appearance of a same T_g event as in cryo QC solid), their DSC heating scans do not exhibit recrystallization events similar to the cryo QC solid, pointing to the differences in the local structure and energetics as compared to the quench-cooled counterpart.

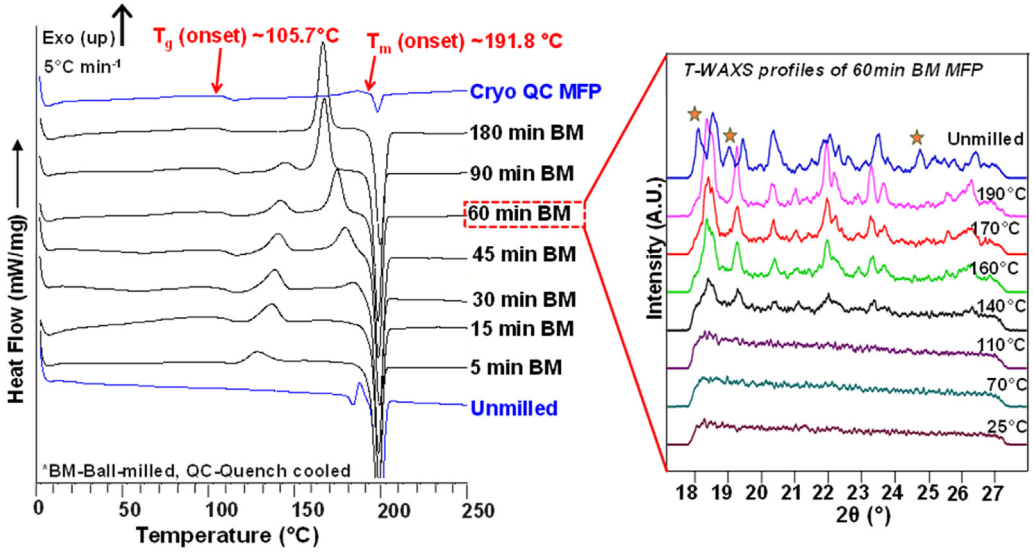

Figure 1. DSC heating curves of cryo-quenched and select ball-milled Mifepristone samples (left) and T–WAXS scan (right) of a 60 min BM MFP. Stars in the T-WAXS plot indicate the additional peaks that correspond to the metastable form in the unmilled MFP sample.

Variable temperature-wide angle X-ray scattering (T-WAXS)

In order to confirm the identities of the recrystallization exotherms observed in DSC scans, a variable temperature WAXS was performed (Fig. 1). To this end, a 60 min BM MFP sample was selected as it demonstrated characteristic double exotherms in DSC. The sample showed a halo diffraction pattern at and under 110°C. Bragg diffraction peaks were first observed at 140°C indicating that nucleation precedes crystal growth. Heating to temperatures above 140°C up to 190°C led to an enrichment of the Bragg diffraction signals, indicating a recrystallization of the amorphous phase. Further, an absence of polymorphic conversion of the residual crystals during heating was confirmed by the enrichment of same Bragg peaks. It is also evident in Fig. 1 that the amorphous fraction is crystallizing into a stable form at 190°C, which is different from the pristine unmilled MFP (as indicated by the presence of Bragg peaks at 2θ = 18.5°, 19.5°, 22.2°).

PXRD and Raman Analyses

The powder X-ray diffraction of unmilled MFP (as received drug), Fig. 2A, indicates intense Bragg diffractions at 2θ 7.84°, which correspond to the Form D, while 10.64°, 11.84°, 16.52° corresponds to Form M. PXRD analysis therefore confirms that the received drug is a mixture of two polymorphs (reported in literature as form M and form D) (shown in supplement Fig. S2).[48] Upon continuing the milling process beyond 60 min, the sample revealed an absence of any Bragg peaks indicating the complete transformation of the solid to an amorphous form with the appearance of a halo.

The Raman spectrum of unmilled crystalline MFP indicates an intense peak at 1590 cm^{-1} with a distinct shoulder at 1614 cm^{-1}. Additionally, a less intense peak also appeared at 1652 cm^{-1}. These bands correspond to the carbonyl and olefinic groups present in the molecule. The ball-milled MFP samples represent a diverse degree of crystalline content as reflected in the differences in intensities in the wavenumber region from 1540–1700 cm^{-1} (Fig. 2B). It can be observed that upon increasing milling durations there is an increase in the relative broadness of the shoulder peak, which eventually merges with the parent peak to become a single broad band above 45 min of milling. There is also an increment in the peak maximum of the intense band from 1590 to 1596 cm^{-1} alongside a shift in the peak at 1652 to 1658 cm^{-1} with increasing milling time. Overall, the appearance of peak broadening with increased milling time is suggestive of the presence of multiple conformations in the solid, hence amorphization.

SEM Characterization

The SEM micrographs exemplified the evolution of the crystal morphology of MFP in the course of milling (Fig. 3). The unmilled MFP represents a combination of smooth surfaced particles with tetragonal prismatic morphology, and irregular small micron sized particles. The stable polymorph of MFP has been reported to exist in the tetragonal prismatic morphology and appear as scattered, however, the metastable form has been reported to contain finer particles which appear more homogenous.[48] It can be observed that milling for 5 min leads to a particle size reduction and, a heterogenous distribution of irregular particles along with ridges that are characteristic of an amorphous state/sites. Upon extending the milling time to 15 min, it seems likely that the particles undergo mechanical fusion and deformation along the cracked plane. The micrograph of 180 min BM MFP contains agglomerated fine particles alternating with protuberances that are reported as characteristic of the amorphous layer.[49]

It can be stated qualitatively from these micrographs that amorphization increases with milling time. Similar evidences of amorphization have also been reported upon milling α-lactose monohydrate.[50] On the other hand, the cryo QC MFP (E) represents smooth and fine irregular plate shaped particles, which could be formed as a result of triturating the quenched glass with a pestle.

Quantification of Crystallinity by Raman Spectroscopy

A partial least square regression (PLS) model was used to quantify the crystallinity in the milled MFP samples. The PLS model described here consists of two principal components (PC). The PC-1 explains 98.0% of the variability in the scores, while PC-2 accounts for 1.56%. A scores plot of Raman spectra of the calibration samples of MFP are shown in Fig. 4. In addition, all scores lie within the Hotelling's T^2 ellipse and no outliers were detected.

An excellent degree of linearity and similarity between the observed and predicted values could be observed as evidenced by R^2=0.9946 and the Q^2=0.9927. Moreover, the model yielded a root mean squared error of estimate (RMSEE)=2.474 as well as a predicted error RMSEP=4.264 (shown in supplement Fig. S3). A slightly high prediction error (RMSEP) of the validation set could be due to the inability of the Raman instrument to discriminate small quantities of amorphous contents above 80% crystallinity in the prepared calibration mixtures. Utilizing this PLS model allowed the crystallinity of the milled MFP samples to be determined (values are shown in supplement Table S1). The unmilled MFP shows a crystallinity value of

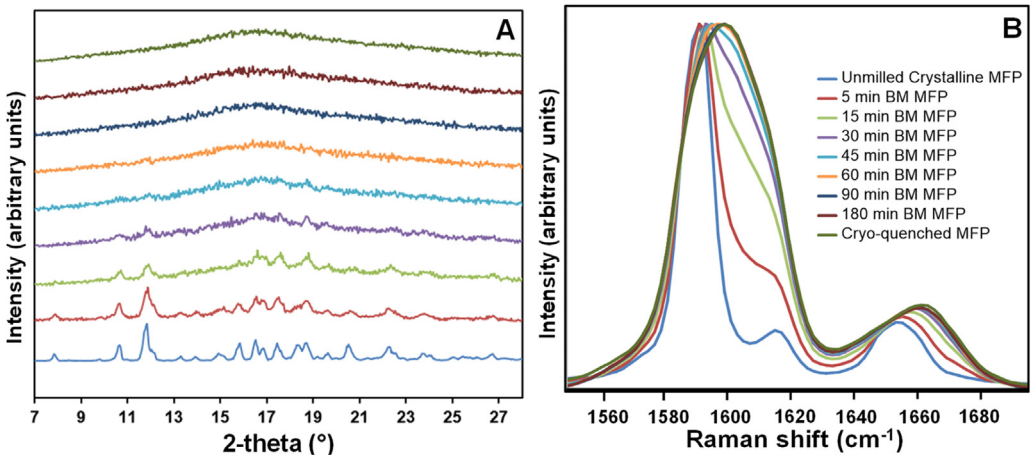

Figure 2. Evolution of amorphization in Mifepristone upon increased ball milling times as evidenced in A. PXRD patterns (reduction in Bragg diffraction peaks) and B. broadening of Raman spectral bands. (Signals are colored according to the legend shown in B). (For interpretation of the references to color in this figure legend, the reader is referred to the web version of this article.)

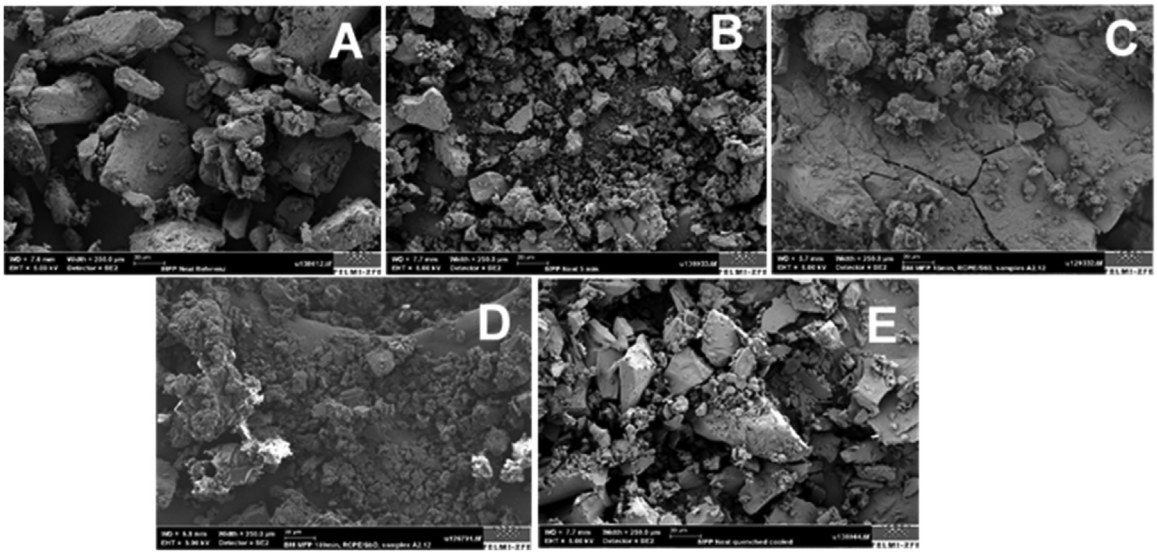

Figure 3. SEM micrographs of unmilled MFP (A), 5 min BM MFP (B), 15 min BM MFP (C), 180 min BM MFP (D) and Cryo QC MFP (E). Scale bars represent 20 μm.

about 95 ± 1%, where the additional ~5 % can be attributed to the presence of two different polymorphs in the received drug.

The model predicts that 5 min milling led to a high degree of amorphization (~55%), which is consistent with PXRD analysis of the same sample, where a sharp reduction in the Bragg diffraction (~50%) was observed. Additionally, milling from 1 to 3 min provides almost a linear decrease in the crystallinity, i.e, around 10% reduction every min. Milling above 30 min sharply reduces the crystallinity (below 7%), and 180 min milling led to a negligible crystallinity (~0.4%) indicating that the sample is almost completely amorphous. Previous results from DSC and PXRD corroborate this finding. It is interesting to note that although the values of crystallinity above 60 min ball milling are below the RMSEE limit (where precision in the predicted values may be questionable) there is a good correlation between the degree of amorphous content to the milled duration. Crystallinity of cryo QC amorphous MFP was about 1.6% which is also consistent with the expectation that the sample is predominantly amorphous. Fig. 5 shows that with an increasing ball milling time, the amorphous content increases in an exponential manner. Such an exponential relationship was previously reported by Descamps et al. to explain amorphization kinetics in Dexamethasone.[51]. Fitting such exponential equation enables one to derive the relaxation time (τ) of the disordering phase. It is known that the glassy state of the amorphous solids constitutes the heterogeneous molecular short-range order, which gradually become more homogenous as a function of time through a process referred to as structural relaxation.[38] We can assume here that such a relaxation is occurring transiently during milling, and competing with the mechanoactivation. The obtained value of τ (5.70 ± 0.11 min^{-1}) indicates that the structural relaxation of MFP can be slower than the collision frequency at 25 Hz (related to mechanoactivation).

Accelerated Stability Outcome

Recrystallization and Degradation Kinetics of MFP. To investigate the (in)stability of the milled MFP samples, accelerated stability studies were carried out at different temperature and relative humidity (RH) conditions. Unmilled MFP was taken as the control sample representing a 'fully' crystalline material. 5- and 15 min BM MFP were chosen as the partially crystalline representatives, and 180 min BM MFP used as the 'fully' amorphous sample. The cryo QC MFP was considered as an alternative amorphous material. Disordered/amorphous materials are metastable in nature and undergo a competitive transformation to the lower energy crystalline state. Since the unmilled MFP as received was found to contain a polymorphic mixture of stable and metastable forms, there was a potential for the metastable form to convert to the stable form upon stability exposure. The PXRD analysis of unmilled MFP sample after 42 d stored under 50°C/45

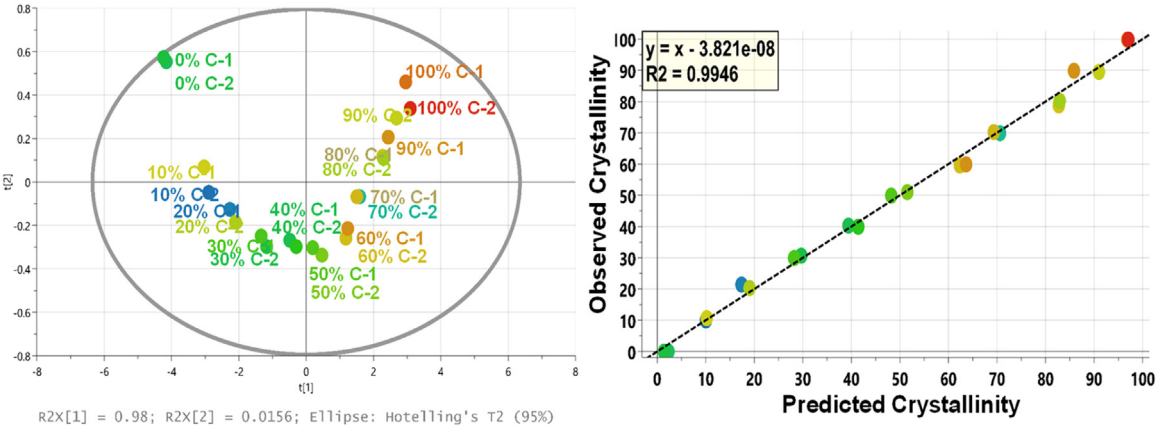

Figure 4. Scores plot of Raman spectra of calibration mixtures (on left) and the PLS-regression (on right) depicting linearity in the observed versus predicted crystallinities.

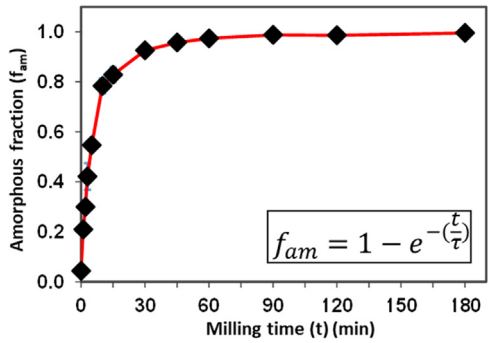

Figure 5. Predicted crystallinity in the milled MFP samples with PLS model and amorphization kinetics. The black dots indicate the measured amorphous fraction and red line shows an exponential fit to data points, as reported previously[51] using the exponential equation shown in the inset box, where τ is the mean relaxation time (min^{-1}).

%RH indicated a reduction in the intensity of the Bragg peaks corresponding to the metastable form and an increase in the Bragg intensity of the stable form (as shown in supplement Fig. S4). Hence, the amount of crystallinity reduced in the unmilled MFP over stability exposure was normalized to 100% and the difference to the observed crystallinity values was added to the all the other samples (as shown in Eq. 4). Fig. 6 shows the kinetics of recrystallization and degradation of different MFP samples.

For 40°C/75 %RH, the recrystallization of samples depended on the initial amorphous content. The 15 min BM MFP shows a faster recrystallization compared to 5 min BM MFP. This behavior can be attributed to the higher degree of amorphous content (hence, possibly the higher molecular mobility) and amorphous-crystalline interfaces in the 15 min BM MFP sample. However, the recrystallization kinetics is slower for 180 min BM MFP, which is interpreted to be caused by a lower nanoscale density heterogeneity as compared to the partially crystalline counterparts. Recent studies have shown that solid-state crystallization is governed by a dynamic interplay of amorphous content and nanoscale density heterogeneity in the sample[52,53] Contrary to this, the cryo QC MFP shows no signs of recrystallization under these conditions. Simultaneous observation of the degradation kinetics of these samples highlight that a higher degradation is observed for the sample consisting of higher initial amorphous content, due to the same hypothesis that the high-energy amorphous fraction is the main reactant for autoxidation, where-as the crystalline counterpart degrades at a negligible rate. At 40°C/10 %RH, there is minimal change in the crystallinity of these samples over 180 d, however, degradation is evidenced in all the samples which follows the previously observed trend i.e., the higher degree of initial amorphous content, the faster it degrades.

Evaluation of recrystallization kinetics at 50°C/75 %RH indicate a similar behavior as that was seen at 40°C/75 %RH, but with an increased rate. The recrystallization kinetics almost appear to converge in the milled samples after 30 d. However, it is noteworthy that the crystallinity of all BM samples never complete to 100%. Moreover, an induction event up to 8 d (where there is no change in the initial crystallinity) is observed for the 180 min BM MFP sample at 50°C/75 %RH. This observation is also consistent with that seen at 40°C/75 %RH. Parallel observation of degradation kinetics in these samples also suggest that the extent of degradation depends on the initial amorphous content, although a greater overlap among the 5- and 15 min BM samples is observed in this case. At 50°C/10 %RH, a reduced overall rate of recrystallization is observed in contrast to that at 50°C/75 %RH. This result is expected as higher humidity has been reported to induce plasticization of the amorphous phase by increasing the molecular mobility.[54]

Recrystallization in all the BM MFP samples at 70°C/75 %RH is extremely rapid. Considering that 70°C/75 %RH represents the harshest conditions used in this stability study, this behavior was not unexpected. It is notable that the 180 min BM MFP recrystallizes quicker than 5- and 15 min BM MFP. Moreover, almost a complete conversion to the crystalline phase can be discerned in the 180 min BM MFP sample at the end of 15 d, compared to the 5- and 15 min BM MFP samples. This behavior is possibly due to a higher molecular mobility in the 180 min BM MFP sample that leads to a faster recrystallization propensity upon storage at such a higher T/%RH. Also, it is interesting to note that a much slower recrystallization is observed for the cryo QC MFP and recrystallization is not complete even at the end of 90 d under these conditions. An important contradiction was notable among the samples stored at 70°C/75 % RH regarding their degradation behavior. The 180 min BM MFP underwent a faster recrystallization in the initial days of exposure (<15 d), and later on degraded to a lower extent in comparison to the 5- and 15 min BM MFP. Moreover, the rest of the samples degraded as per the remaining residual amorphous fraction with the cryo QC MFP sample degrading to almost about 3.5% at the end of 90 d.

Subsequent observations of recrystallization kinetics for MFP samples exposed at 70°C/10 %RH also indicate recrystallization (albeit much slower than at 70°C/75 %RH) where, the crystallinity of all BM samples converges to 80% at the end of 30 d. Likewise, their extent of degradation also converges and becomes comparable after 30 d exposure at 70°C/10 %RH. The cryo QC MFP is more resistant to recrystallization and degrades to a much higher extent (~6%) at the end of 90 d under these conditions.

Based on the above observations, the following inference can be drawn regarding the disorder in the MFP samples. A faster recrystallization was observed for samples stored under elevated %RH compared to those at lower %RH. Both elevated %RH and temperature are factors which affect the recrystallization. The dominant factor depends on how close to the T_g is the amorphous phase under a given stability exposure. Moreover, factors leading to an overall high molecular mobility of the amorphous phase led to recrystallization. A cryo QC MFP can exist at a higher energy landscape compared to the 180 min BM MFP, as the former was generated from the fused molten state, while the latter was generated by inducing a continuous crystal lattice disorder. The “memory effect” of (nano) crystallites or nuclei reminiscent in the BM amorphous samples could contribute as seeds to facilitate further nucleation and crystal growth. A similar observation was also reported for ursodeoxycholic acid where the cryo-quenched amorphous solid remained amorphous even after seeding with the crystals, while the grounded material underwent crystallization upon exposure to ethanol vapors.[55]

The degree of crystallinity in the milled MFP samples has a definite relationship to the disordered phase undergoing degradation (autoxidation). A higher degree of degradation was overall witnessed at lower %RH. This can be attributed to the presence of higher amounts of amorphous fraction remaining in the samples at lower %RH, owing to a minimal to negligible competitive recovery due to recrystallization. The unmilled ‘pristine’ crystals degrade to a lesser extent than the milled samples at all the conditions, which confirms that the amorphous phase is predominantly degrading.

Moisture Sorption and Desorption Behavior. To investigate the moisture sorption behavior of the amorphous samples, a DVS analysis was performed. A comparison of moisture sorption behavior of the milled amorphous (180 min BM MFP), cryo QC amorphous MFP, and the unmilled crystalline MFP is shown in the Fig. 7.

For the crystalline/unmilled MFP, there is minimal difference between the moisture sorbed and desorbed cycle, with a maximum moisture gained at 90 %RH less than 0.1%. However, for the 180 min BM MFP (milled amorphous), 1.83% moisture is gained at 90 %RH which is typical for amorphous solids (as amorphous solids normally

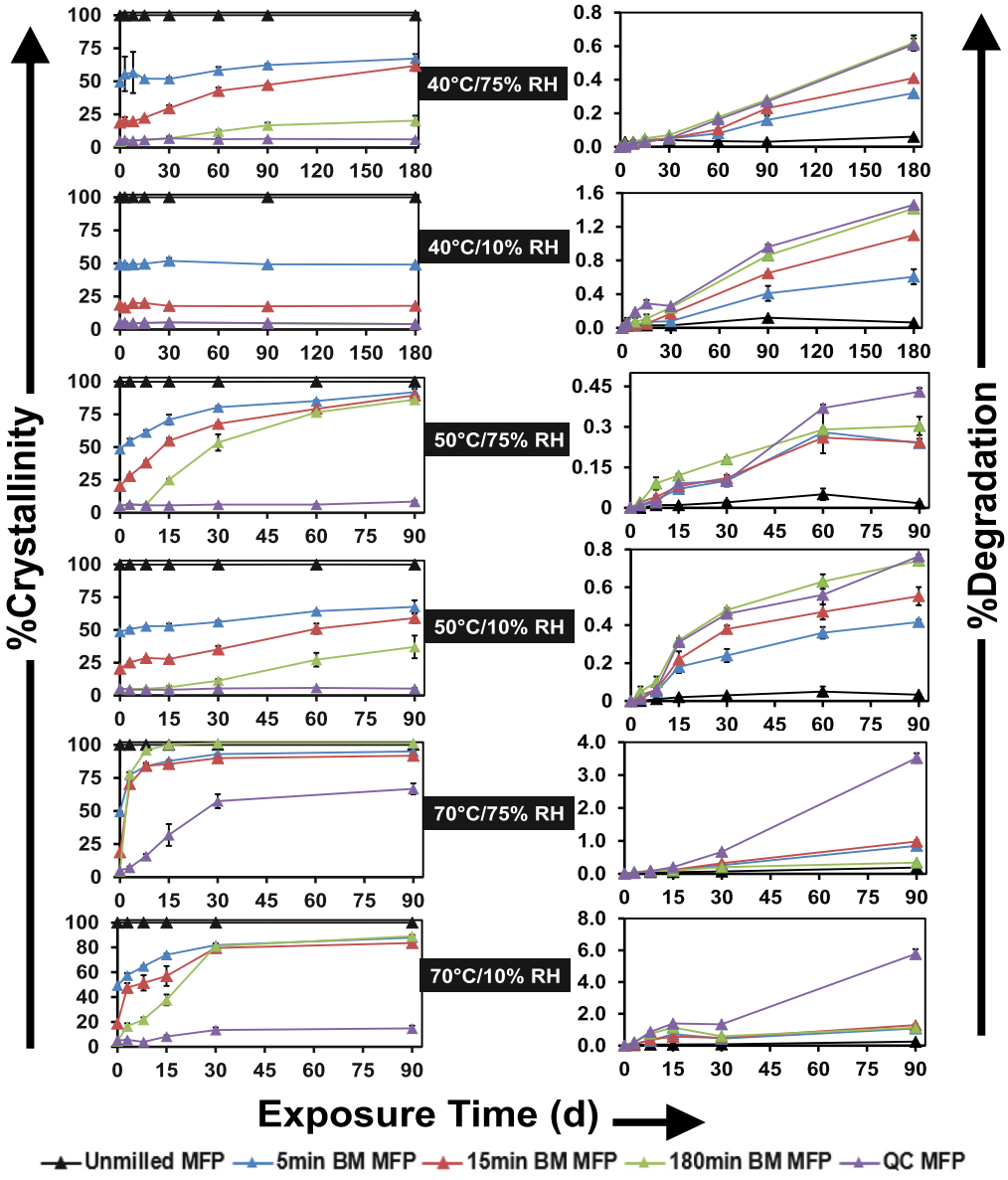

Figure 6. Plots demonstrating recrystallization kinetics (on the left) and degradation kinetics (on the right) of Mifepristone samples containing different degree of disordered content, stored under different accelerated stability conditions. Colored triangles represent the average value while error bars demonstrate standard deviation of individual samples (n = 3). Colored lines are for visual aid only. (For interpretation of the references to color in this figure legend, the reader is referred to the web version of this article.)

sorb up to 10–20% more moisture than crystals). In addition, the hysteresis of desorption isotherm is consistent with the plasticization of amorphous phase. The samples were evaluated at 25°C and the reports are expected to be the 'equilibrium moisture' gain.

It can also be observed that the moisture sorbed by 180 min BM MFP is higher than the cryo QC MFP. A possible explanation for this is ascribed to the amorphization resulting from accumulation of crystal defects in the milled sample enhancing the free-volume for stronger moisture–solid interaction thereby facilitating absorption.[56] The degree of hysteresis observed in the cryo QC MFP is lower than 180 min BM MFP, which implies a reduced tendency for the quenched amorphous solid to undergo plasticization.[57,58]

In addition to the DVS evaluation, the moisture gained in the samples exposed to accelerated stability exposure was also evaluated by gravimetry. Fig. S5 (supplement), shows higher moisture gain correlates with higher amorphous content, however, higher observed errors and overlap impede an accurate interpretation. The moisture gain trend at 50°C/75 %RH are consistent with an initial higher moisture uptake of the amorphous sample followed by a decrease in the overall gain. This initial moisture gain is sustained for a longer time for the samples exposed at 40°C/75 %RH as compared to the ones exposed at 50°C/75 %RH. The decreasing moisture levels could be attributed to the recrystallization (which is faster for the samples exposed at 50°C/75 %RH as compared to 40°C/75 %RH). The rate of moisture gain therefore competes with recrystallization of the amorphous phase during the stability exposure. Moreover, for cryo QC MFP, the extent of weight loss is much slower compared to the BM samples, which is in line with previous observation. The maximum moisture gain determined gravimetrically was 1.6 ± 0.5 %w/w for the cryo QC MFP and 1.4 ± 0.5 %w/w for the 180 min BM MFP. These values are in good agreement with the 'equilibrium moisture gained' by the sample under DVS analyses.

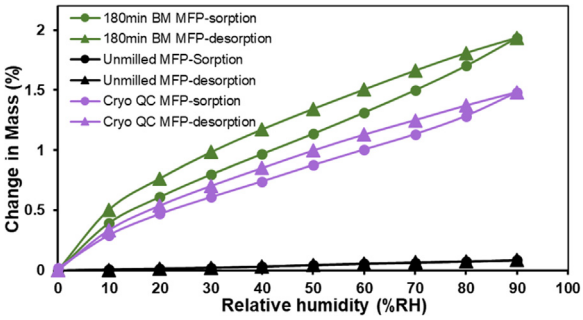

Figure 7. DVS sorption-desorption isotherms for crystalline and amorphous MFP samples at 25°C.

Plasticization and annealing effects. The high energy and hygroscopic amorphous phases in milled solids can undergo plasticization upon the moisture sorption. Water increases the molecular mobility of the amorphous phase thereby leading to a reduction in T_g.[59] To evaluate the degree of plasticization in the milled MFP sample, DSC analyses was performed in a hermetically sealed pan to identify a 'wet T_g' for the 180 min BM MFP sample.

A representative 180 min BM MFP sample was selected as this sample sorbed the highest amount of moisture (~1.83 %w/w) upon exposure at 40°C/75 % RH for 30 d. Fig. 8 shows the thermal events observed in the sample. The total heat flow scan reveals a depression in the T_g value and an appearance of a recrystallization exotherm and a melting endotherm. The zoomed inset presents the corresponding reversing heat flow signal comparing the T_g profiles of unexposed and exposed sample. The exposed sample has a T_g value 83.6°C, while that of the unexposed sample is 105.6°C indicating the plasticization of the amorphous phase due to water sorption. The theoretical T_g value of the sample with the given moisture fraction obtained from the Fox eq. ($T_{gmix}^{-1} = w_{MFP}{*}T_{gMFP}^{-1}+w_{water}{*}T_{gwater}^{-1}$, where w is the respective weight fraction) was found to be 93.9°C. This indicates that there can be a non-ideal mixing interaction of the sorbed water with amorphous MFP in the plasticized state, elevating the mobility. Fig. S5 (shown in the supplement) compares the gravimetric moisture sorption kinetics of the samples exposed at 40°C/ 75 %RH and at 50°C/75 %RH. It can be seen that the trend in sorption kinetics of amorphous samples is comparable across these temperatures for the level of moisture sorbed. Since the chosen stability conditions were

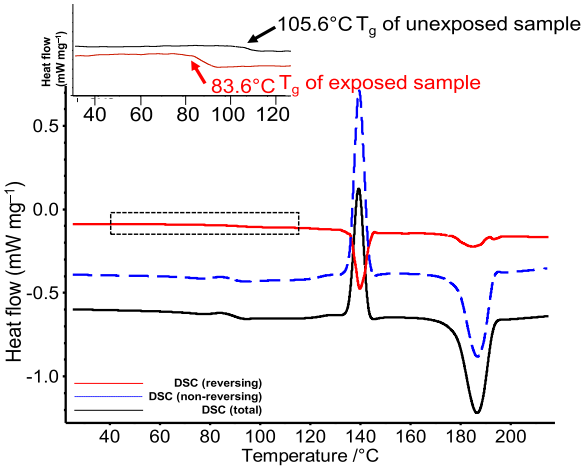

Figure 8. DSC heating curves (recorded using the hermetically sealed pans) of 180 min BM MFP exposed to 40°C/75 %RH for 30 d highlighting the influence of plasticization on T_g onset. The zoomed inset compares the T_g onset of an unexposed 180 min BM MFP sample to that of this exposed sample in a reversing mode (by modulated DSC).

overall lower than the plasticized T_g, it can be presumed that these samples degrade in the glassy state (below T_g) under these conditions.

Samples exposed at 70°C/75 %RH were also analyzed to evaluate if the recrystallization was complete, and to determine the impact of annealing on the disordered state. Fig. 9 highlights an overlay comparison of heating scans (DSC) of the milled and amorphous MFP samples exposed at 70°C/75 %RH for different durations. The influence of annealing of the crystal disorder accompanied with (ordering) recrystallization in the milled MFP samples is clearly observed. Increasing the exposure times from 0 d (unexposed) to 30 d results in a drastic reduction in the enthalpy of recrystallization in all the milled samples indicating that the amorphous fraction reduces over time. For the 5- and 15 min BM MFP samples, the change in recrystallization exotherm is almost comparable after 8 d, consistent with the observed extent of recrystallization in these samples. However, for the 180 min BM MFP sample, a drastic decrease in the recrystallization enthalpy (alongside a shift in the recrystallization onset temperature) is evidenced. This phenomenon is related to the higher molecular mobility in this sample as compared to the partially crystalline MFPs. Also, the drastically reduced recrystallization enthalpy for the 180 min BM MFP sample is attributed to its higher degree of crystallinity within the first 8 d of exposure (Fig. 6)

A distinct T_g (in reversing flow) was not possible to distinguish in these samples probably due to the temporal decrease of amorphous content, and an increased interference from sorbed water. Yet, small quantities of amorphous phase were even preserved until the end of such a long-term harsh exposure (30 d). Moreover, the recrystallization is not complete in any of these milled samples even at the end of 30 d at 70°C/75 %RH exposure, which poses an interesting question about the evolution of crystal defects in pharmaceutical solids. It can be acknowledged that identifying factors, which could heal these crystal defects, will have important repercussions to stability.

The thermogram of cryo QC MFP reveals striking differences in the crystallization and annealing behavior. A distinct T_g is observed in a freshly cryo QC MFP sample which undergoes remarkable relaxation as apparent from the sharp enthalpy recovery over the course of storage at 70°C/75 %RH. The enthalpic relaxation undergoes random shifts in its onset temperature over the course of exposure alongside the change in the onset of melting. The latter could be due to the formation of oxidative degradants. In addition, the recrystallization exotherm preceding the melting endotherm persists at the end of 30 d indicating the sample's partly crystalline nature.

Replication of Experiments at Multiple Sites. The competition observed among recrystallization and degradation rates is important, yet there is a missing link in understanding the degradation of amorphous solids. With a purview of examining the reproducibility of these phenomena in MFP, Pfizer U.K. Ltd and AstraZeneca Inc. conducted the studies under diverse stability conditions using the protocol outlined in section "*Accelerated Stability Evaluation*".

Fig. 10 shows the degradation and recrystallization kinetics for selected samples milled at and below 15 min. These results present trends similar to that seen before.

The recrystallization rates systematically increase over time; being faster for samples milled for higher duration (more amorphous). It can be observed that the recrystallization rates are much slower for the samples exposed to 40°C/75 %RH, as compared to those at 50°C/75 %RH, which is consistent with the higher molecular mobility at 50°C facilitating the recrystallization. However, a significant difference in the recrystallization rates cannot be observed among the samples exposed to 50°C/75 %RH and 50°C/45 %RH. It follows from two conditions that the milled samples attain a similar crystallinity at the end of 28 d, as these values coincide. The samples with higher amorphous content degraded to a higher extent which is

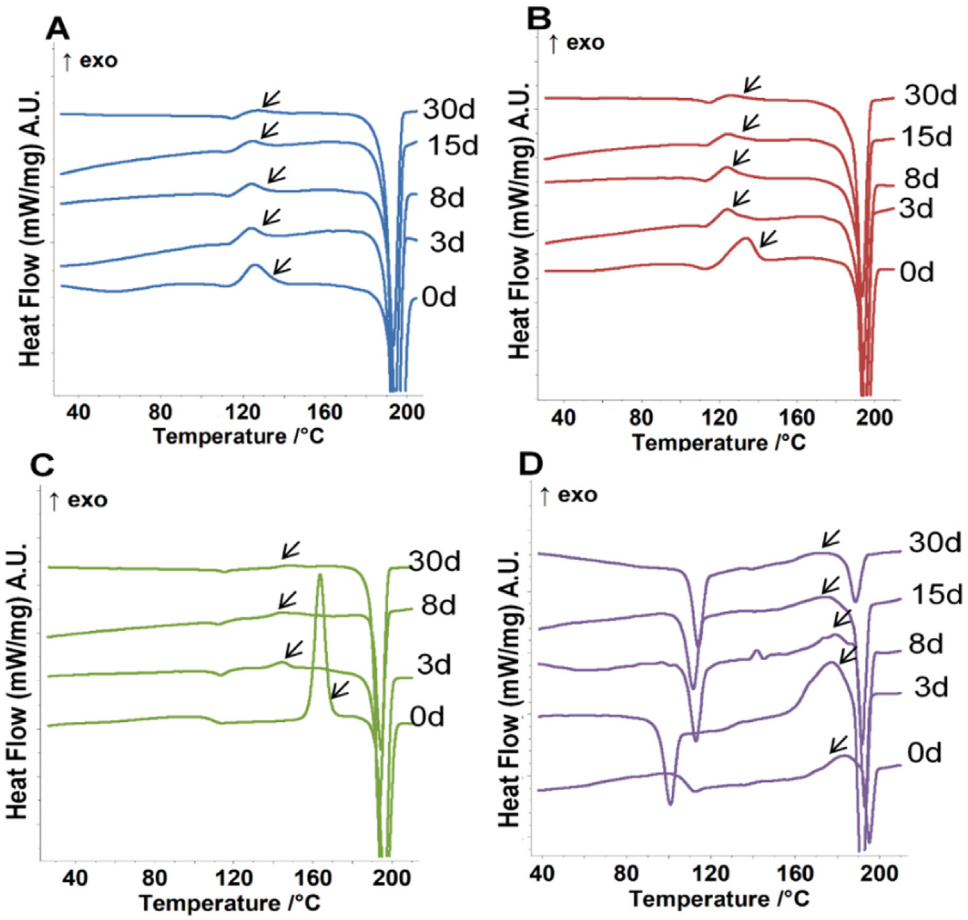

Figure 9. Overlaid DSC thermograms indicating the annealing and recrystallization of disordered MFP samples upon exposure to 70°C/75 %RH for different days (d). A, B, C and D represent the 5-, 15-, 180 min BM MFP, and cryo QC MFP respectively. Black arrows point to the changes in recrystallization exotherm.

analogous with our previous observation (Fig. 6). The samples exposed to 50°C/75 %RH degrade higher than the ones at 40°C/75 %RH, and almost equivalent to the ones exposed at 50°C/45 %RH. A possible explanation to this event is attributed to the presence of remaining amorphous content (that has not undergone recrystallization). To summarize, a competition between recrystallization and degradation was observed here, and their rates (and the extents) were comparable to that shown in Fig. 6. Noteworthy here is that the recrystallization rates are generally higher than the degradation rates, signifying the inherent propensity of MFP is to crystallize.

Fig. 11 depicts the comparison of recrystallization and degradation kinetics of MFP samples examined at AstraZeneca Inc. No change in the crystallinity was observed for the majority of the samples at 40°C/10 %RH. There was also minimal to no change in the crystallinity of samples exposed under 40°C/75 %RH as well, contrary to our previous findings. A possible reason for this behavior could be associated with ageing of the milled sample. Ageing of milled solids under humid conditions has been reported to reduce the surface energies and enhance their physical stabilities.[37,60,61] The approximate time between the day the solids were milled and the day the solids were exposed under stability conditions, in this case, was 150–180 d, which could have an impact on reducing the surface free-energy and the molecular mobility. Before exposing to stability studies, the milled solids were stored in a refrigerator at 5°C. The influence of ageing of the milled trehalose has been described by Descamps et al.[62] where, sub-T_g annealing at 70°C, rendered an overall increase in the onset temperatures of the (sub-T_g) endotherm corresponding to molecular relaxations. Due to the absence of recrystallization event at 40°C/75 %RH, the degradation values are comparatively higher to that observed in Fig. 6.

On the other hand, the samples exposed under 70°C undergo recrystallization where the kinetics is faster at 75 %RH as compared to 10 %RH. A similar trend in the competition between the recrystallization and degradation compared to results in Fig. 6 is observed in the milled samples, where the degradation is faster at lower %RH, owing to the competitive recovery of crystallinity at higher %RH.

Elucidation of Degradation Mechanism. MFP was found to undergo autoxidation resulting in the same degradants in solid-state stress (RapidOxy®) as that were formed in solution stress study (using AIBN as the stressor). Moreover, a major additional degradation peak is observed in solution stress study (AIBN) which is attributed to the hydroxylated product of MFP similar to that reported for metabolite investigations in MFP.[63] A control solution (devoid of AIBN) exposed under the same stress conditions (50°C/5 h) did not indicate any degradants. This implies that the drug solution is chemically stable under the exposed conditions. However, the free radicals generated from AIBN decomposition causes autoxidation. Common degradants formed under solution- and solid-state stress studies for the above-mentioned samples and a cryo QC MFP exposed for 90 d at 70°C/10 %RH are labelled from a–d in the chromatogram Fig. 12. The structures of these degradants were assigned based on their accurate and tandem mass spectra. The mass spectrum of individual autoxidation products is shown in Supplement (Fig. S7). The N-demethylated MFP (a) was the major degradant (0.91 RRT) formed in all the BM MFP samples under accelerated stability conditions. However, N-di-

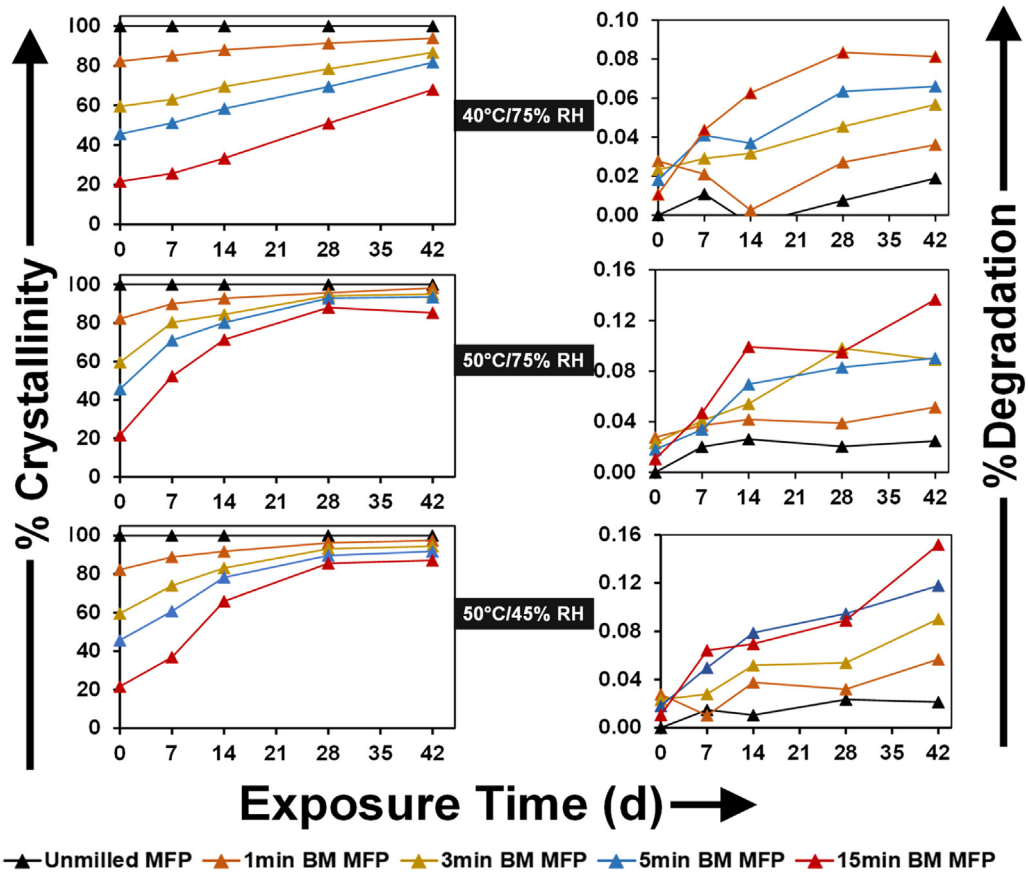

Figure 10. Plots demonstrating recrystallization kinetics (on the left) and degradation kinetics (on the right) of MFP samples. Colored lines are for the visual aid only. (Experiments were conducted at Pfizer U.K. Ltd). (For interpretation of the references to color in this figure legend, the reader is referred to the web version of this article.)

demethylated degradant (b), and a N-hydroxylated product (c) was also formed in minor quantities upon extended storage. These products were already reported previously.[63] Another minor degradant (d) results from the abstraction of H-atom from hydroxylated demethylated MFP.

The formation of these degradants can be accelerated in a short period of time by exposing the solid samples to high pressure O_2 gas i.e. RapidOxy® (700 kPa O_2/100°C/2 d) which is consistent with our previous observation.[64] Moreover, the absence of these degradants in the control sample exposed under N_2 gas in RapidOxy® (700 kPa N_2/100°C/2 d) confirms that the degradation mechanism involves autoxidation (i.e. the presence of O_2 is a prerequisite), and that the same high pressure and high temperature without oxygen is unable to induce reaction. Fig. 12B indicates the mechanism of demethylation which might occur in the solid-state. A free-radical mediated autoxidation mechanism is proposed for the formation of demethylated products, where it is postulated firstly that ball-milling MFP generates free-radicals (as a consequence of amorphization) that reacts with molecular oxygen (in air). The subsequent steps involve bond-rearrangement resulting in the elimination of methyl group. These steps are expected to repeat in tandem thereby leading to the formation of di-demethylated MFP.

Kinetic Modelling of the Stability Data. As presented in Fig. 6, unmilled (crystalline) MFP presented minimal degradation during stability testing compared to milled (disordered) samples. As accelerated stability-based methods for predicting the degradation of pristine crystalline solids already exist, the primary focus here is on modelling the degradation of disordered MFP solids. Normalizing the degradation values with respect to the amorphous fraction in the preceding stability time point provided an effective degradation value which was fitted with a diffusion model (Eq. 6) to extract the degradation rate constants (Table 4**)**. A general trend of increased degradation with increased amorphous content can be ascertained using this table. The 70°C/75 %RH data was not considered here as there was a drastic reduction in the amorphous content to 0% within the first few days of exposure. It is thus recognized that this approach can only be useful to model the degradation, where the recrystallization is not complete. Also, harsh conditions can result in secondary degradation.

A natural logarithm was applied to the autoxidation rate constants (supplement Table S2). Application of the extended Arrhenius eq. (Eq. 7) was extended by surface fitting the degradation rate points, providing a good fit (R^2 above 0.95) in all the cases (Fig. 13). Here, the selection was limited to 4 conditions: 40°C/10 %RH, 40°C/75 %RH, 50°C/10 %RH and 50°C/75 %RH. This excluded the harsher 70°C conditions. The surface fitting allowed extraction of the respective Arrhenius kinetic triplet ln A, E_a, and B, which were used to calculate the degradation rate at 25°C/60 %RH. The degradation profile of samples stored under 25°C/60 %RH is shown in the supplement Fig. S8.

Table 5 shows a strong correlation between the predicted and actual degradation rates for the milled samples. Predicting the degradation for the fully amorphous MFP samples, however is more challenging. Moreover, the B-term (humidity sensitivity parameter) is negative indicating an inverse correlation to the degradation. This result emphasizes that moisture-induced recrystallization competes with degradation. Additional validation of the model predictions was made by eliminating conditions where recrystallization was observed and attempting to predict the degradation rates of samples at those

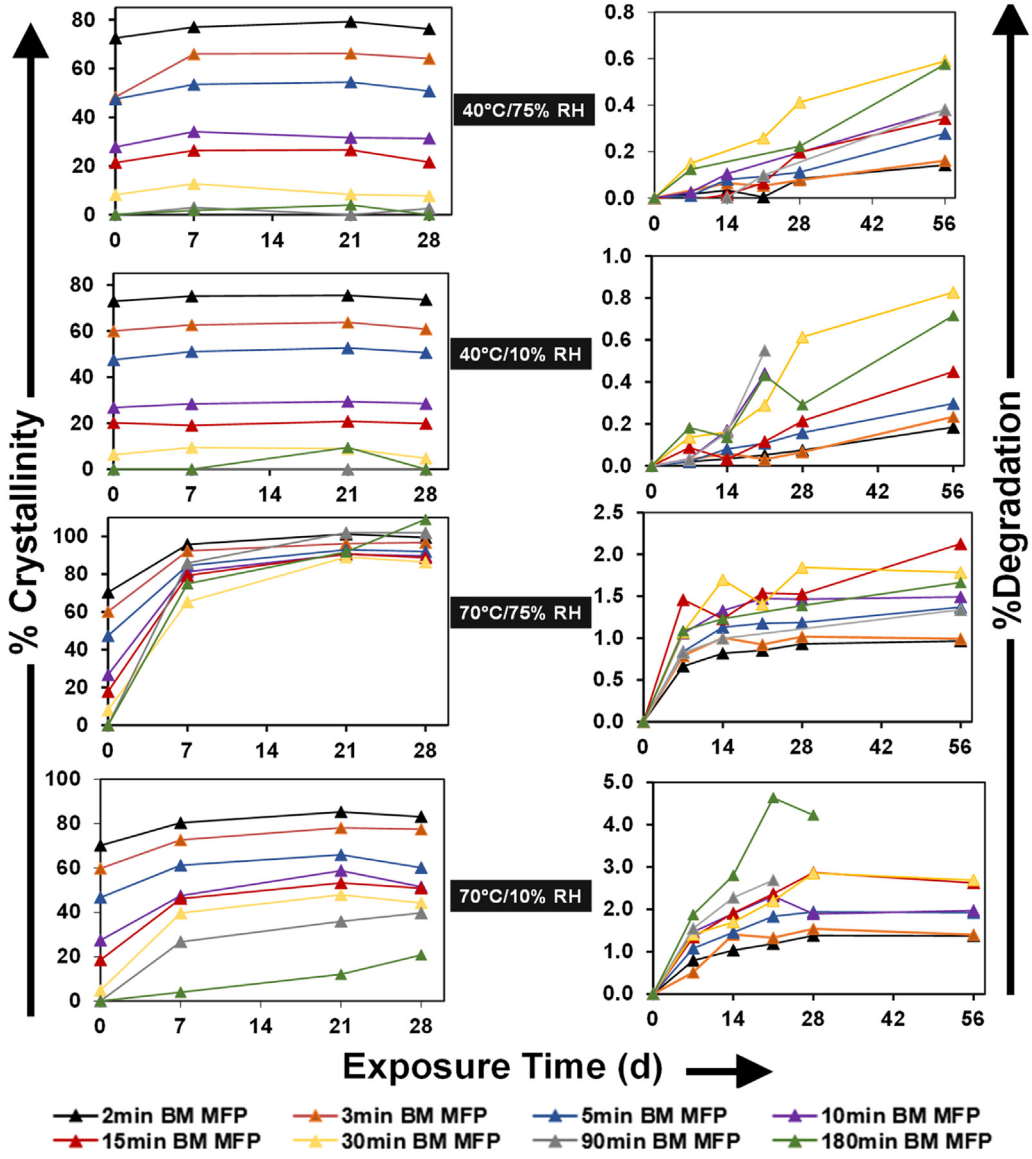

Figure 11. Plots depicting recrystallization kinetics (on right) and degradation kinetics (on left) of MFP samples. Colored lines are for the visual aid only. (Experiments were conducted at AstraZeneca Inc.) (For interpretation of the references to color in this figure legend, the reader is referred to the web version of this article.)

eliminated conditions. A good degree of similarity between the predicted and actual values are observed for the partially crystalline sample (Fig. 14).

Fig. 14 shows the predicted degradation rates are increasing for samples as a function of their initial amorphous content, therefore, samples with higher amorphous content undergo a higher degradation under the exposed conditions. However, cryo QC MFP appears as an exception, where the plausible differences in the dynamics of the amorphous state appears to be complicate the accurate predictions.

Results similar to that described above were also attained by modelling degradation kinetics (with diffusion equation fitted) and applying the modified Arrhenius equation by AstraZeneca Inc. (using the experimental data shown in Fig. 11). Here, the use of highly aged samples resulted in a flat recrystallization trend under most of the exposure conditions except 70°C/75 %RH. In the latter case, sufficient model fits (based on diffusion model) were obtained even without normalizing for the amorphous content (data shown in supplement Fig. S10 and Table S3). A possible explanation to the excellent surface fits is due to the absence of recrystallization of MFP samples under most of the conditions.

Discussion

Amorphization of MFP During Ball Milling

The as-received MFP was initially characterized by multiple solid-state analytical techniques: DSC, PXRD, FTIR, and Raman spectroscopies. Although the data from DSC and Raman measurements could only indicate the presence of a metastable polymorph of MFP, PXRD and ATR-FTIR were sensitive enough to detect the presence of a polymorphic mixture. The as received MFP (unmilled) was considered as a crystalline reference for determining the crystallinity of milled samples. Thermal analysis of BM MFP indicated that the amorphous content increases with the milling time (as shown by the increasing levels of recrystallization enthalpies). The recrystallization kinetics of milled MFP solids depicted a progressive development of exotherms upon milling for longer durations as was also shown in the case for, Dexamethasone.[51] Moreover, the shifting of onsets of the recrystallization event to temperatures with progressive milling time indicates the stabilizing nature of milled amorphous state which is consistent with the previous report[17] (Fig. 1, Fig. S3). As shown in supplement

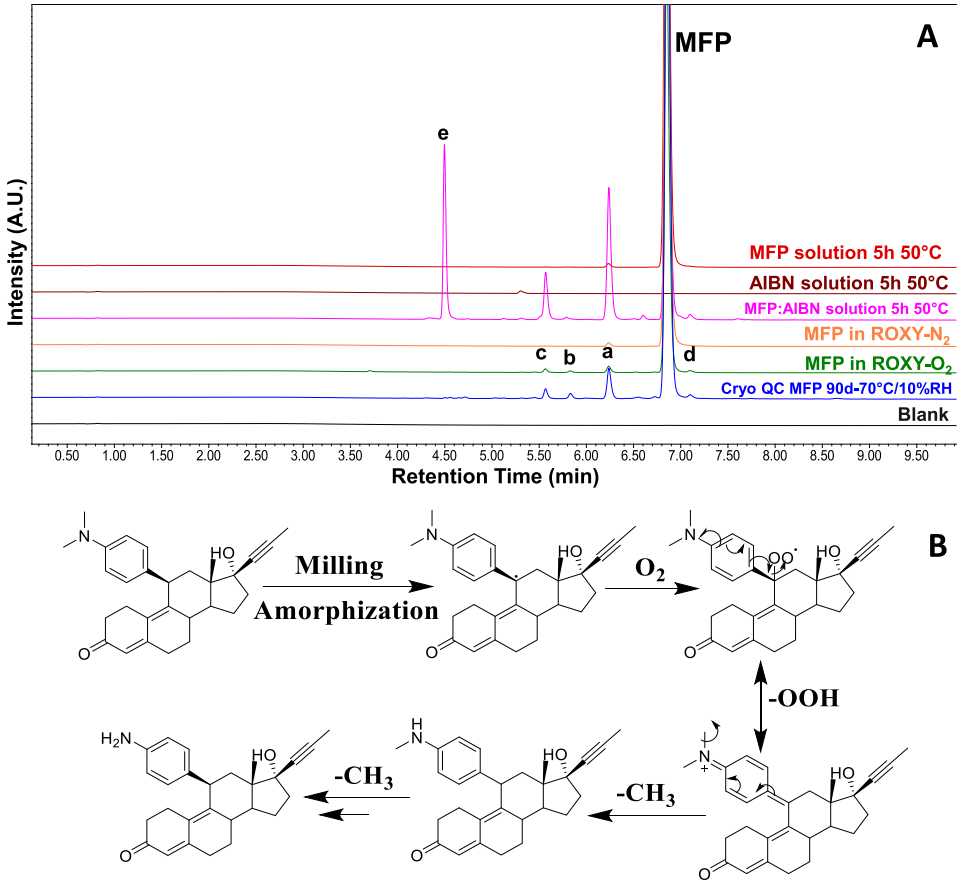

Figure 12. A. Stacked chromatogram highlighting the similarity of MFP-autoxidation degradants formed under solution and solid-state stress studies as well as under accelerated storage and B. Proposed mechanism of demethylation by autoxidation of MFP. (ROXY-RapidOxy®).

Fig. S3, the samples milled below 5 min do not evidence a T_g, thus any form of disorder generated is expected to be predominantly at the crystal surface. The recrystallization exotherm observed in these samples can be attributed to the reorganization of the crystal defects (possibly at the surface) to more ordered crystals. It appears that milling at- and above 5 min leads to the accumulation of excess defects, attesting a T_g of amorphous phase in the thermograms. For samples milled above 30 min, a dual exothermic response was observed. Investigation of these exotherms (60 min milled MFP) indicated an enrichment of Bragg diffraction signals that precludes any polymorphic transformation. However, it could be seen that the enriched Bragg signals (corresponding to recrystallization of the amorphous fraction) are different to the pristine (as received) MFP crystals. In addition, a single melting event corresponding to the stable polymorph was recorded for these milled samples in DSC. These findings may suggest that the recrystallization of a stable polymorph of MFP from the amorphous (milled) solid is linked to both surface- and bulk recrystallization occurring in the supercooled liquid state. Trasi et al.[65,66] evidence dual exotherms in several cryo-milled solid drugs (*e.g.* Piroxicam, Griseofulvin) to be attributed to the surface- and bulk recrystallization phenomena, respectively. The former being faster occurs at relatively lower temperatures. Interestingly, for the 180 min BM MFP, only a single exotherm (in DSC) was observed, which could suggest the occurrence of concomitant surface- and bulk crystallization. A similarity in the recrystallization and melting enthalpies of 180 min BM MFP suggests that the sample has recrystallized during the DSC run which is otherwise fully amorphous as prepared. The cryo QC MFP also evidenced a T_g similar to the milled samples indicating its vitreous nature.

PXRD analysis did not reveal any change in the existing polymorph, rather it showed a reduction in the Bragg diffraction peaks upon increasing milling times, indicating amorphization. A similar

Table 4
Extracted autoxidation rates for disordered MFP samples.

Temperature (°C) ± 1°C	Relative humidity (%RH) ±5%	Degradation rate constants of MFP samples shown as mean ± standard error (n = 3) *10^3			
		5min BM (d^{-1})	15min BM (d^{-1})	180min BM (d^{-1})	Cryo QC (d^{-1})
40	10	2.7 ± 0.2	4.2 ± 0.6	11.4 ± 0.5	17.7 ± 1.6
40	75	1.0 ± 0.1	1.7 ± 0.1	3.5 ± 0.2	5.7 ± 0.3
50	10	1.8 ± 0.7	6.0 ± 1.7	12.2 ± 2.7	21.9 ± 2.8
50	75	1.4 ± 0.4	2.3 ± 0.8	4.2 ± 1.7	10.8 ± 1.0
70	10	12.0 ± 0.6	33.8 ± 2.9	39.1 ± 8.6	127.0 ± 8.6
25	60	1.7 ± 0.2	4.1 ± 0.3	5.9 ± 0.5	1.1 ± 0.2

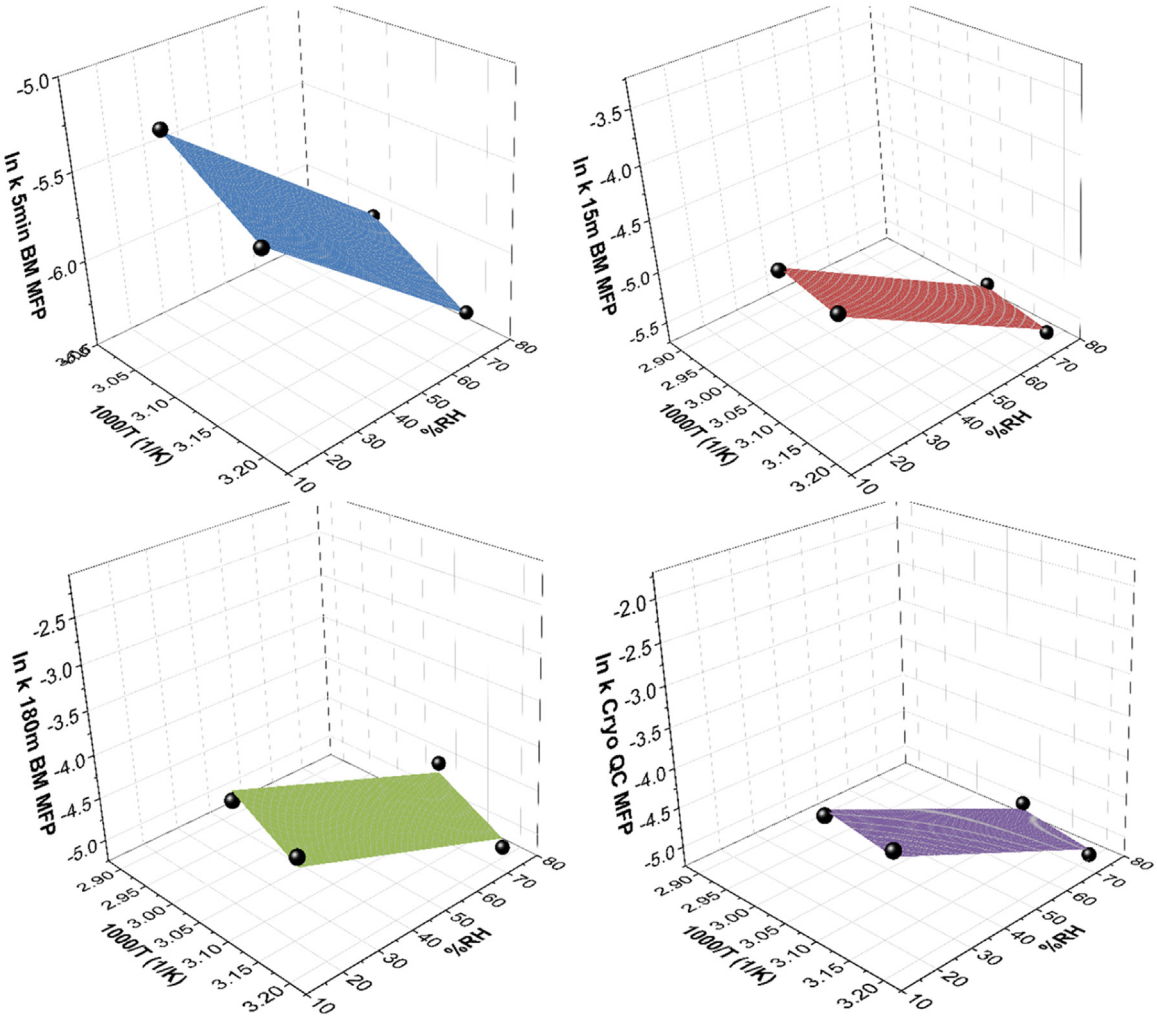

Figure 13. Application of extended Arrhenius equation (Eq. 8) to generate the fitted surface plots. A goodness of fit (R^2) of >0.95 was obtained in all the cases.

inference was supported with Raman and FTIR spectroscopic measurements (Fig. 2). Descamps et al. have reported that milling a solid above the T_g of its amorphous phase usually results in polymorphic transformation, while milling below the T_g induces amorphization.[67,68] Considering that Bragg peaks for the milled samples do not differ in this study, it can be said that the powder during milling would have a temperature lower than the T_g i.e. <105°C.

Assessment of the Degree of Disorder and Amorphization

Key factors need to be considered while selecting a technique for evaluating the degree of crystallinity in the milled solids based on sensitivity to polymorphic transformation, interferences from moisture or other contaminants/degradants, and discrimination between the crystalline or amorphous phases.

Raman spectroscopy was considered appropriate due to its non-destructive nature allowing us to retain the same samples after analysis. We found comparable crystallinity by PXRD and Raman method for a 5 min BM MFP (data not shown). Ideally, the crystallinity from the Raman method needs to be cross validated with PXRD technique for entire crystallinity level. However, owing to the small sample quantity, sampling time, and throughput requirements, Raman method was preferred. Also, unlike DSC, the Raman method does not involve heating hence, it can be expected to retain the original crystallinity and the physical state of the sample. Raman calibration samples represent a two-phase physically mixed system as compared to the one-phase disordered system. However, owing to the indifference between the Raman spectrum of the 180 min BM MFP sample and that of the cryo QC MFP sample, we believe the differences in predicted crystallinity values would be negligible. The 180 min BM

Table 5
Derived Arrhenius parameters (by surface fitting) used to predict degradation under 25°C/60 %RH and comparison to the actual degradation rates at 25°C/60 %RH. Standard errors are shown for the predicted and actual degradation rates.

Samples	Ln A	E_a/R	B ($\%^{-1}$)	Ln k	Predicted $k_{25°C/60\ \%RH}$ (d^{-1}) x 10^3	Actual $k_{25°C/60\ \%RH}$ (d^{-1}) x 10^3
5mim BM MFP	5.61	6.74	−0.015	−6.70	1.20 ± 0.04	1.70 ± 0.20
15mim BM MFP	−0.34	2.40	−0.019	−5.54	3.90 ± 0.04	4.10 ± 0.30
180mim BM MFP	9.85	6.79	−0.015	−5.52	4.00 ± 1.00	5.90 ± 0.50
Cryo QC MFP	1.47	3.19	−0.020	−5.13	5.90 ±1.00	1.10 ± 0.20

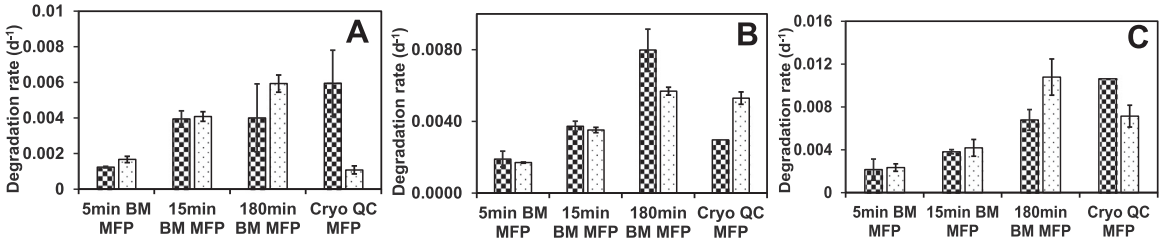

Figure 14. Comparison of the predicted and actual degradation rates for MFP samples containing different degrees of disorder stored at A: 25°C/60 %RH, B: 40°C/75 %RH, and C: 50°C/75 %RH. Black spotted bars (filled) indicate the predicted degradation rate and the empty bar with fine dots indicates the actual/observed degradation rates. The error bars denote the standard error in the fitted parameters.

MFP was considered as the reference amorphous in order to simulate the particle effects of milled samples. A good R^2 and low RMSEE score were obtained in the calibration samples which supports the utility and performance of this model for evaluating the crystallinity. Multivariate analysis of the Raman spectra of the milled MFP samples was evaluated with a generated PLS model that illustrated the exponential nature of the amorphization kinetics. This observation is consistent with the reports on milling induced amorphization kinetics observed for Dexamethasone[51] and Sulfathiazole.[69] For MFP, a dramatic amorphization proceeds within the first 5 min of ball milling (about 50 %) (supplement Fig. S3), as evidenced by a sharp difference in the vibrational bands in Raman spectra. Interestingly, the DSC analysis revealed much higher crystallinity value for the same 5 min BM MFP sample (data not shown). This is expected in the presence of crystal defects as they still need energy to break the remaining crystal lattice interactions upon melting thus leading to similar fusion enthalpy as that of the crystal (hence higher crystallinity).[70] The mDSC analysis (supplement Fig. S3) did not reveal a distinct T_g in the samples milled below 5 min, rather exotherms corresponding to recrystallization were observed, which suggest that the milled solids predominantly consist of surface crystal defects.

Investigation of (in)Stabilities

Following the identification of crystallinity in the milled samples, the next objective was to subject the samples to accelerated storage conditions. Owing to the higher molecular mobility in the milled (disordered) crystals, such solids have been commonly reported to undergo physical transformation (recrystallization). A commonly held notion is that an amorphous solid prepared by undercooling a melt undergoes recrystallization at much reduced rate as compared to the milled counterparts. This is because of the presence of residual seed (crystals) present in the milled solids that facilitates a "memory effect" which is expected to be absent in the melt quenched solid. On the other hand, several reports have highlighted the higher chemical degradation of an amorphous solid as compared to its crystalline counterpart, where a reasonable correlation exists among the molecular mobility to their degradation (rates or extent). The works published previously from our group have investigated the differences in nanoscale density heterogeneity in the milled solids.[52] The invariant-Q obtained from small angle X-ray scattering (SAXS) quantifies the density heterogeneity and is related to the entropy of the system. A relationship was observed between the nanoscale density heterogeneity and autoxidation for disordered Simvastatin.[53] Considering the above-mentioned aspects, we believe that a competition exists between the recrystallization and degradation phenomena in amorphous (milled) solids upon storage that is driven by the molecular mobility. The investigation of crystallinity (via Raman) and degradation (via LC) was performed on the same sample to minimize any variations. Under accelerated stability conditions, the recrystallization rate of milled MFP was considerably faster than that of the degradation rate. The slopes of the degradation curves were proportional to the initial amorphous content in the milled MFP samples, which signifies a relationship of higher amorphous content to a faster and higher extent of degradation. The cryo QC MFP was the slowest to recrystallize hence, the fastest to degrade. Interestingly, the extent of recrystallization was never complete under any of the conditions, which implies that the residual amorphous content underwent degradation. The control crystalline sample (unmilled MFP) degraded to a much lower extent (<0.1%) under the accelerated conditions which testifies that the amorphous counterpart is indeed degrading. Assessment of particle sizes of the MFP samples was carried out over the course of a representative stability exposure (40°C/75 %RH) (supplement Fig. S6). It was expected that upon exposure to elevated humidity, the particle size would increase as a result of agglomeration formed due to water bridges.[71] However, contrasting reports have highlighted anomalous behavior of particle size reduction of milled particles upon stability exposures where, the claimed mechanism involved 'stress-relaxation' of milled particles driving particle de-aggregation.[72] Here an insignificant change in the mean particle size (D_{50}) (supplement Fig. S6) meant that no trends in the particle sizes are visible. Thus, it can be concluded that a higher degradation in MFP is truly a result of amorphous contents.

Investigation of the moisture sorption potential of the 180 min BM MFP and the cryo QC MFP (Fig. 7) indicated that the former sorbs a higher moisture amount. This could be due to the presence of crystal defects, hence larger free energy and free volume. However, considering that the amorphous steroidal molecule is hydrophobic (log P ~4.5),[73] the degree of sorption is typically not more than 2%. This finding has an implication on the plasticization of the amorphous phase. It was noted for a sample with the highest moisture (~1.8%), that the plasticization of amorphous phase resulted in a reduction of T_g (by ~20°C) yet, MFP is expected to degrade and recrystallize from the glassy state under the accelerated stability conditions. Investigation of annealing the crystal defects at higher temperature and %RH (70°C/75 %RH) (with DSC) did not indicate a completion of recrystallization in any of the samples. Rather, it appears that the amorphous phase experiences a 'fractal effect' (rigid arrangement of amorphous clusters in a way that reduces further crystallization-induction by an overall reduction in the mobility, free volume, and moisture percolation) at a higher (85–90%) crystallinity, after which the recrystallization rates are negligible (Fig. 10). Here, the samples milled below 5 min (low degree of disorder) show the same trend of increasing degradation with higher initial amorphous content.

Examination of the major degradants emerging in the accelerated stability studies indicated them to be demethylated and di-demethylated products of MFP. Oxidative dealkylation have been reported to occur in amines in the solution state.[74] We propose a mechanism where amorphization results in the formation of free radicals that initiate subsequent steps of autoxidation. The formation of free-radicals as a result of mechanoactivation or processing has been previously reported.[75,76] A comparison of the degradants formed in the solid

state with that of the solution stress study conducted with AIBN also reflects a similarity that corresponds to the free-radical based autoxidation mechanism.

Kinetic Modelling of Degradation Accounting Crystallization

The commonly used solid state degradation prediction technique is based on the application of extended Arrhenius equation (factoring in the humidity) such as accelerated stability assessment program (ASAP). Although such a model is widely recognized in the pharmaceutical industry for evaluating degradation of crystalline solids, limited cases of use are reported for situations where a change to the solid state occurs. Here, we make an investigational attempt to model solid state degradation (autoxidation) by accounting for the recrystallization of disordered solids. An important feature of competition between recrystallization and degradation in such solids is described here, and is analogous to the report for intramolecular cyclization of Gabapentin.[77] The choice of selected accelerated temperature and humidity conditions was such that the samples are stored below the 'wet T_g' of amorphous fractions. An initial inspection of degradation kinetics factored with respect to their amorphous content (at preceding time point) indicated that selecting extreme conditions (e.g., temperatures above T_g−50°C) may present modelling difficulties due to propagation of errors while interpolating to long-term conditions. Application of diffusion model was shown to approximate the degradation kinetics (autoxidation) in all the samples (supplement Fig. S7), although a slight non-linearity was observed as expected for solid state degradation. In cases where competitive recrystallization occurs, the degradation kinetics tapers off over the exposure time and may show deviations from the fit. Therefore, limiting the kinetic time points to lower exposure times has been proposed, which is analogous to the iso-conversion approach that assumes linearity over those exposure times.

An inspection of Arrhenius surface fit to the actual degradation rates (un-normalized with respect to preceding amorphous content shown in the supplement Fig. S9), did not indicate a good fit (R^2<0.9) for the samples undergoing concomitant crystallization. However, normalizing degradation rates to the preceding amorphous content led to an excellent Arrhenius (surface) fit (Fig. 13). A decent correlation among the predicted and actual reaction rates was observed for the 5- and 15 min BM MFP samples under long-term stability conditions (where the samples do not recrystallize) as well as under conditions, where recrystallization was observed. Degradation predictions were within the standard errors for the 180 min BM MFP sample stored under long-term stability conditions. However, they deviated under accelerated conditions. It is reported that molecular mobility of the amorphous phase might be a major contributor to both recrystallization and degradation.[38,78] Studies have highlighted that, differences in the nature and origin of molecular motions depend on storage time and temperature.[79] It is recognized in this work that depending on the amount and plasticization of amorphous phase present in the sample, their recrystallization dynamics largely differ. The presented approach to model degradation therefore cannot be used in conditions where the sample has completely recrystallized. Otherwise, the degradation values fall to zero, due to zero amorphous content. The degradation kinetics of replication experiments performed at Pfizer could not be modeled owing to the limited studied conditions (as a minimum of 4 points are required for applying a surface fit). Nonetheless, the degradation kinetics of experiments performed at AstraZeneca indicated an excellent Arrhenius surface fit (shown in supplement Fig. S10) and allowed determination of the shelf-life of the milled solids (shown in supplement Table S3). Considering that the milled samples were annealed over the time they were loaded to stability, the amorphous phase tends to remain physically stable. This could explain why a surface fit was possible even without normalizing for the preceding amorphous content. In the cases where the amorphous phase prefers to recrystallize, normalizing the actual degradation rates seems to improve the fits.

Scope and Opportunities of Present Work

Opportunities in improving the outcome of presented semi-empirical model can include the identification and exploration of molecular factors contributing to differences in degradation. Although, the present study was carried out to understand the role of differing amorphous contents on the chemical stability (autoxidation) of MFP, a clear opportunity remains in exploring the influence of molecular mobility on the storage stability of the drug. Considering both degradation and recrystallization rates have been shown to depend on the molecular mobility, we believe that studying the change in molecular mobility over the time of stability exposure could be factored into the development of robust predictive stability models. In addition, the implication of (unintentionally) varied hold time between fresh milling to loading the stability batches was shown to alter the recrystallization rates, hence, the degradation (Fig. 11). Interestingly, the extent of degradation increased for MFP solid that presumably annealed over the course of storage (did not evidence recrystallization) (Fig. 11). Examination of surface free energies of milled MFP solids over the course of fresh milling and during extended storage could provide additional clues about the relationship among the surface free energy−recrystallization−molecular mobility that could shed insights into its degradation behavior. Although annealing has been proven to improve the physical stability of drugs, its influence on autoxidation remains to be explored. The answers to these complex solid-state phenomena driven by molecular dynamics are at least not straightforward, and will appeal to the upcoming research possibilities existing unexplored in this domain integrating deep material science principles. Secondly, ample opportunities exist in quantifying the disorder (low level, <1−5%) by microscopic techniques, apart from conventional techniques. Taken together, it seems promising that the development of sensitive techniques in quantifying the change in disorder (or amorphous content) over stability storage, alongside the investigation of molecular dynamics (molecular mobility) holds further promises in developing a robust solid-state stability by design paradigm.

Conclusions

This study was envisaged to understand the influence of crystal disorder on the autoxidation of a model drug (MFP). The selected drug has a high T_g and underwent amorphization/crystal disorder upon ball milling at room temperature which followed an exponential behavior as reported for many other drugs.[35,51] The milled samples were characterized by different solid-state techniques which indicated different degree of crystallinity depending on the milled duration. Subjecting MFP samples with different degree of amorphous content (with fully amorphous and fully crystalline MFP samples as controls) under accelerated stability conditions evidenced a competition between recrystallization and degradation. The mechanism of degradation in the solid-state was similar to that occurring in solution state stress study (AIBN as the stressing agent), proving it to be autoxidation. Demethylated products were primarily formed in the solid samples stored under the accelerated stability conditions. Crystallinity in the samples was quantified using a Raman-PLS model. Samples containing a higher initial amorphous content degraded to a higher extent under the stability conditions, thus implying a correlation. By normalizing the degradation behavior of the disordered samples with respect to their amorphous content (in preceding timepoint) the degradation kinetics could be fit to a diffusion model (as oxygen diffusion has been known to be rate limiting to induce

autoxidation). Extracting the autoxidation rate constants for conditions with and without recrystallization allowed an application of surface fit (with extended Arrhenius equation) that enabled prediction of the degradation kinetics of milled solids at long-term storage conditions. An exception to successfully predicting the degradation rate was observed for the fully amorphous (180 min BM MFP and cryo QC MFP) samples, which was rationalized as an effect of the rapid change in the amorphous dynamics, faltering the predictions. Such a semi-empirical model could therefore be useful in predicting the degradation in samples with partial crystallinity as might occur for samples that are commonly subjected to processing conditions (sieving, milling, blending, compaction, drying, etc.); however, for the fully amorphous samples deconvolution of the effects of molecular dynamics in the amorphous state needs further investigation.

Declaration of Interests

The authors declare that they have no known competing financial interests or personal relationships that could have appeared to influence the work reported in this paper.

Acknowledgment

The authors thank partners of the Stability by Design (SbD) consortium partners (Pfizer, AstraZeneca, UCB, Janssen, and FELMI) for co-funding this work, and are grateful to Patricia Basford, Thomas Dane, and Paul Whiteside (Pfizer, U.K.), Samantha Fairhurst, Sara Ryan, Charlotte Bennett, Stephanie Brookes (AstraZeneca, U.K.), Luc Aerts and Kristina Kassner (UCB), and Hana Prokopcova (Janssen) for the scientific discussions and suggestions. We thank FELMI ZFE, Graz (Austria), for the analysis of powder X-ray diffraction samples. This work was funded through the Austria COMET Program by the Austrian Federal Ministry of Climate Action, Environment, Energy, Mobility, Innovation, and Technology, the Austrian Federal Ministry of Labour and Economy, the Federal State of Styria, and SFG. The COMET Program is managed by the Austrian FFG. Acknowledgements also go to Michael Brunsteiner for discussions related to this topic and to the RCPE team for their support and research facilities.

Supplementary Materials

Supplementary material associated with this article can be found in the online version at doi:10.1016/j.xphs.2023.03.020.

References

1. Bajaj S, Singh S, eds. *Methods for Stability Testing of Pharmaceuticals*. New York: Springer; 2018. https://doi.org/10.1007/978-1-4939-7686-7.
2. ICH Q1A(R2). *International Conference on Harmonization (ICH). Guidance for Industry: Q1A(R2) Stability Testing Of New Drug Products And New Drug Substances*. 4. 200320032003:24.
3. Qiu F, Scrivens G. *Accelerated Predictive Stability*. Elsevier; 2018. https://doi.org/10.1016/B978-0-12-802786-8.00001-2.
4. Fu M, Perlman M, Lu Q, Varga C. Pharmaceutical solid-state kinetic stability investigation by using moisture-modified Arrhenius equation and JMP statistical software. *J Pharm Biomed Anal*. 2015;107:370–377. https://doi.org/10.1016/j.jpba.2015.01.014.
5. Gabrič A, Hodnik Ž, Pajk S. Oxidation of drugs during drug product development: problems and solutions. *Pharmaceutics*. 2022;14(2). https://doi.org/10.3390/pharmaceutics14020325.
6. Waterman KC, Adami RC, Alsante KM, et al. Stabilization of pharmaceuticals to oxidative degradation. *Pharm Dev Technol*. 2002;7(1):1–32. https://doi.org/10.1081/PDT-120002237.
7. Kotha RR, Zhang K, Yehl P, Kumar A. Oxidative degradation in pharmaceuticals: mechanism and stabilization of a spray-dried amorphous drug – a case study. *J Pharm Biomed Anal*. 2022;220(February): 114962. https://doi.org/10.1016/j.jpba.2022.114962.
8. Clancy D, Hodnett N, Orr R, Owen M, Peterson J. Kinetic model development for accelerated stability studies. *AAPS PharmSciTech*. 2017;18(4):1158–1176. https://doi.org/10.1208/s12249-016-0565-4.
9. Singh S, Junwal M, Modhe G, et al. Forced degradation studies to assess the stability of drugs and products. *TrAC Trends Anal Chem*. 2013;49:71–88. https://doi.org/10.1016/j.trac.2013.05.006.
10. Waterman KC. The application of the accelerated stability assessment program (ASAP) to quality by design (QbD) for drug product stability. *AAPS PharmSciTech*. 2011;12(3):932–937. https://doi.org/10.1208/s12249-011-9657-3.
11. Parrott EL. Pharmaceutical sciences milling of pharmaceutical solids. *J Pharm Sci*. 1974;63(6):813–829.
12. Li M, Azad M, Davé R, Bilgili E. Nanomilling of drugs for bioavailability enhancement: a holistic formulation-process perspective. *Pharmaceutics*. 2016;8(2). https://doi.org/10.3390/pharmaceutics8020017.
13. Vemuri NM, Brown AB, Authelin J-R, Hosek P. *Milling Process for the Production of Finely Milled Medicinal Substances*. 1999. Published online June.
14. Shah UV, Olusanmi D, Narang AS, et al. Decoupling the contribution of surface energy and surface area on the cohesion of pharmaceutical powders. *Pharm Res*. 2015;32(1):248–259. https://doi.org/10.1007/s11095-014-1459-3.
15. Abouhakim H, Quayle MJ, Norberg ST, et al. Mechanically induced amorphization of diaqua-bis(omeprazolate)-magnesium dihydrate. *Cryst Growth Des*. 2020;20(9):6057–6068. https://doi.org/10.1021/acs.cgd.0c00770.
16. Müller T, Krehl R, Schiewe J, Weiler C, Steckel H. Influence of small amorphous amounts in hydrophilic and hydrophobic APIs on storage stability of dry powder inhalation products. *Eur J Pharm Biopharm*. 2015;92:130–138. https://doi.org/10.1016/j.ejpb.2015.03.006.
17. Feng Tao, MTC Rodolfo Pinal. Process induced disorder in crystalline materials differentiating defective crystals from the amorphous form of Griseofulvin. *J Pharm Sci*. 2008;97:3207–3221. https://doi.org/10.1002/jps.21219.
18. Begat P, Young PM, Edge S, Kaerger JS, Price R. The effect of mechanical processing on surface stability of pharmaceutical powders: visualization by atomic force microscopy. *J Pharm Sci*. 2003;92(3):611–620. https://doi.org/10.1002/jps.10320.
19. Vippagunta RR, LoBrutto R, Pan C, Lakshman JP. Investigation of metformin HCl lot-to-lot variation on flowability differences exhibited during drug product processing. *J Pharm Sci*. 2010;99(12):5030–5039. https://doi.org/10.1002/jps.22207.
20. Iyer J, Brunsteiner M, Modhave D, Paudel A. Role of crystal disorder and mechanoactivation in solid-state stability of pharmaceuticals. *J Pharm Sci*. 2023. https://doi.org/10.1016/j.xphs.2023.02.019. Published online February.
21. Saraf I, Modhave D, Kushwah V, et al. Feasibility of rapidly assessing reactive impurities mediated excipient incompatibility using a new method: a case study of famotidine-PEG system. *J Pharm Biomed Anal*. 2020;178: 112893. https://doi.org/10.1016/j.jpba.2019.112893.
22. Ueyama E, Suzuki N, Kano K. Mechanistic study of the oxidative degradation of the triazole antifungal agent CS-758 in an amorphous form. *J Pharm Sci*. 2013;102(1):104–113. https://doi.org/10.1002/jps.
23. Baertschi SW, Brunner H, Bunnell CA, et al. Isolation, identification, and synthesis of two oxidative degradation products of olanzapine (LY170053) in solid oral formulations. *J Pharm Sci*. 2008;97(2):883–892. https://doi.org/10.1002/jps.
24. Giovanni B, Deleuze C, Gachon M, Palmisano G, Vergnaud JP. Autoxidation of tetrazepam in tablets: Prediction of degradation impurities from the oxidative behavior in solution. *J Pharm Sci*. 1992;81(2):183–185. https://doi.org/10.1002/jps.2600810216.
25. Kanaujia P, Poovizhi P, Ng WK, Tan RBH. Preparation, characterization and prevention of auto-oxidation of amorphous sirolimus by encapsulation in polymeric films using hot melt extrusion. *Curr Drug Deliv*. 2019;16(7):663–671. https://doi.org/10.2174/1567201816666190416123939.
26. Aoki M, Nishimura H, Mimura A, Kita S, Yasuzawa T, Terada K. Identification of the degradation products of the steroid sulfatase inhibitor KW-2581 in jet mill-micronized powder. *J Pharm Sci*. 2013;102(6):1760–1772. https://doi.org/10.1002/jps.
27. Schenck L, Neri C, Jia X, et al. A co-processed API approach for a shear sensitive compound affording improved chemical stability and streamlined drug product processing. *J Pharm Sci*. 2021;110(9):3238–3245. https://doi.org/10.1016/j.xphs.2021.05.013.
28. Makoto O, Nobuyoshi K. Effect of grinding on the crystallinity and chemical stability in the solid state of cephalothin sodium. *Int J Pharm*. 1990;62(1):65–73. https://doi.org/10.1016/0378-5173(90)90031-X.
29. Otsuka M, Kaneniwa N. Effect of environment on crystallinity and chemical stability in solid state of ground cephalothin sodium during storage. *Drug Dev Ind Pharm*. 1991;17(7):909–918.
30. Fujita M, Himi S, Handa T. Effects of compression and grinding on chemical stability of a benzodiazepine receptor agonist. *Chem Pharm Bull*. 2010;58(1):51–55. https://doi.org/10.1248/cpb.58.51.
31. Ikeda Y, Ban J, Ishikawa T, Hashiguchi S, Urayama S, Horibe H. Stability and stabilization studies of TAK-599 (ceftaroline fosamil), a novel N-phosphono type prodrug of anti-methicillin resistant Staphylococcus aureus cephalosporin T-91825. *Chem Pharm Bull*. 2008;56(10):1406–1411. https://doi.org/10.1248/cpb.56.1406.
32. Pas T, Bergonzi A, Michiels E, et al. Preparation of amorphous solid dispersions by cryomilling: chemical and physical concerns related to active pharmaceutical ingredients and carriers. *Mol Pharm*. 2020;17(3):1001–1013. https://doi.org/10.1021/acs.molpharmaceut.9b01265.
33. Adrjanowicz K, Kaminski K, Grzybowska K, et al. Effect of cryogrinding on chemical stability of the sparingly water-soluble drug furosemide. *Pharm Res*. 2011;28(12):3220–3236. https://doi.org/10.1007/s11095-011-0496-4.
34. Šagud I, Zanolla D, Perissutti B, Passerini N, Škorić I. Identification of degradation products of praziquantel during the mechanochemical activation. *J Pharm Biomed Anal*. 2018;159:291–295. https://doi.org/10.1016/j.jpba.2018.07.002.

35. Elisei E, Willart JF, Danède F, Siepmann J, Siepmann F, Descamps M. Crystalline polymorphism emerging from a milling-induced amorphous form: the case of chlorhexidine dihydrochloride. *J Pharm Sci*. 2018;107(1):121–126. https://doi.org/10.1016/j.xphs.2017.07.003.
36. Abdul-Fattah AM, Dellerman KM, Bogner RH, Pikal MJ. The effect of annealing on the stability of amorphous solids: chemical stability of freeze-dried moxalactam. *J Pharm Sci*. 2007;96(5):1237–1250. https://doi.org/10.1002/jps.20947.
37. Puri V, Shur J, Narang AS. Elucidating molecular-and particle-level changes during the annealing of a micronized crystalline drug. *Mol Pharm*. 2019;16(10):4339–4351. https://doi.org/10.1021/acs.molpharmaceut.9b00692.
38. Shamblin SL, Hancock BC, Pikal MJ. Coupling between chemical reactivity and structural relaxation in pharmaceutical glasses. *Pharm Res*. 2006;23(10):2254–2268. https://doi.org/10.1007/s11095-006-9080-8.
39. Sumie Yoshioka YA. Correlations between molecular mobility and chemical stability during storage of amorphous pharmaceuticals. *J Pharm Sci*. 2007;96:960–981. https://doi.org/10.1002/jps.
40. Tamura K, Ono M, Kawabe T, Yonemochi E. Impact of magnesium stearate content: modeling of drug degradation using a modified arrhenius equation. *Chem Pharm Bull*. 2020;68(11):1049–1054. https://doi.org/10.1248/cpb.c20-00443.
41. Patterson A, Ferreira AP, Banks E, et al. Modelling drug degradation in a spray dried polymer dispersion using a modified Arrhenius equation. *Int J Pharm*. 2015;478(1):348–360. https://doi.org/10.1016/j.ijpharm.2014.11.063.
42. Naveršnik K. A simple non-linear kinetic model to evaluate stability of a pressure sensitive drug. *J Pharm Sci*. 2022;111(11):3108–3113. https://doi.org/10.1016/j.xphs.2022.07.010.
43. Robnik B, Likozar B, Wang B, Ljubin TS, Časar Z. Understanding and kinetic modeling of complex degradation pathways in the solid dosage form: the case of saxagliptin. *Pharmaceutics*. 2019;11(9):1–21. https://doi.org/10.3390/pharmaceutics11090452.
44. Baertschi SW, Jansen PJ, Alsante KM, Santafianos D, Harmon P, Boccardi G, Baertschi SW, Alsante KM, Reed RA. Chapter 2. Stress testing: a predictive tool. Chapter 3. Stress testing: the chemistry of drug degradation. Chapter 6. Oxidative susceptibility testing. 2nd ed. *Pharmaceutical Stress Testing- Predicting Drug Degradation*. 23. USA: Informa Healthcare; 2011:104–105. Inc.169.
45. Scrivens G. *Predicting the Long-Term Stability of Solid-State Pharmaceuticals ASAP (Accelerated Stability Assessment Program): Theory, Limitations and Applications*. 2015. March.
46. Khawam A, Flanagan DR. Solid-state kinetic models: basics and mathematical fundamentals. *J Phys Chem B*. 2006;110(35):17315–17328. https://doi.org/10.1021/jp062746a.
47. Qiu Z, Stowell JG, Morris KR, Byrn SR, Pinal R. Kinetic study of the Maillard reaction between metoclopramide hydrochloride and lactose. *Int J Pharm*. 2005;303(1-2):20–30. https://doi.org/10.1016/j.ijpharm.2005.06.016.
48. Xu J, Gong XF, Li P, Chen XF, Wang HP, Ning LF. Mifepristone polymorph with enhanced solubility, dissolution and oral bioavailability. *Steroids*. 2020;159:108649. https://doi.org/10.1016/j.steroids.2020.108649.
49. Bruni G, Berbenni V, Sartor F, et al. Quantification methods of amorphous/crystalline fractions in high-energy ball milled pharmaceutical products. *J Therm Anal Calorim*. 2012;108(1):235–241. https://doi.org/10.1007/s10973-011-1504-y.
50. Badal Tejedor M, Pazesh S, Nordgren N, et al. Milling induced amorphisation and recrystallization of α-lactose monohydrate. *Int J Pharm*. 2018;537(1-2):140–147. https://doi.org/10.1016/j.ijpharm.2017.12.021.
51. Oliveira PFM, Willart JF, Siepmann J, Siepmann F, Descamps M. Using milling to explore physical states: the amorphous and polymorphic forms of dexamethasone. *Cryst Growth Des*. 2018;18(3):1748–1757. https://doi.org/10.1021/acs.cgd.7b01664.
52. Laggner P, Paudel A. Density fluctuations in amorphous pharmaceutical solids. Can SAXS help to predict stability? *Colloids Surf B*. 2018;168:76–82. https://doi.org/10.1016/j.colsurfb.2018.05.003.
53. Modhave D, Laggner P, Brunsteiner M, Paudel A. Solid-state reactivity of mechano-activated simvastatin: atypical relation to powder crystallinity. *J Pharm Sci*. 2019;108(10):3272–3280. https://doi.org/10.1016/j.xphs.2019.05.032.
54. Hancock BC, Zografi G. The relationship between the glass transition temperature and the water content of amorphous pharmaceutical solids. *Pharm Res An*. 1994;11(4):471–477. https://doi.org/10.1023/A:1018941810744.
55. Yonemochi E, Inoue Y, Buckton G, Moffat A, Oguchi T, Yamamoto K. Differences in crystallization behavior between quenched and ground amorphous ursodeoxycholic acid. *Pharm Res*. 1999;16(6):835–840. https://doi.org/10.1023/A:1018817801444.
56. Newman A, Zografi G. An examination of water vapor sorption by multicomponent crystalline and amorphous solids and its effects on their solid-state properties. *J Pharm Sci*. 2019;108(3):1061–1080. https://doi.org/10.1016/j.xphs.2018.10.038.
57. Vrentas JS, Vrentas CM. Hysteresis effects for sorption in glassy polymers. *Macromolecules*. 1996;29(12):4391–4396. https://doi.org/10.1021/ma950969l.
58. Argatov I, Kocherbitov V. An empirical model for sorption by glassy polymers: an assessment of thermodynamic parameters. *Polym Test*. 2021;99: 107220. https://doi.org/10.1016/j.polymertesting.2021.107220.
59. Feng T, Stanciu L, Carvajal M. Making sense of milling: the role of water on the micro-structural relaxation-like of cryo-milled griseofulvin. *Water*. 2012;4:18–36. https://doi.org/10.14294/WATER.2012.3.
60. Ohta M, Buckton G. Determination of the changes in surface energetics of cefditoren pivoxil as a consequence of processing induced disorder and equilibration to different relative humidities. *Int J Pharm*. 2004;269(1):81–88. https://doi.org/10.1016/j.ijpharm.2003.08.015.
61. Newell HE, Buckton G, Butler DA, Thielmann F, Williams DR. The use of inverse phase gas chromatography to study the change of surface energy of amorphous lactose as a function of relative humidity and the processes of collapse and crystallisation. *Int J Pharm*. 2001;217(1-2):45–56. https://doi.org/10.1016/S0378-5173(01)00589-0.
62. Descamps M, Aumelas A, Desprez S, Willart JF. The amorphous state of pharmaceuticals obtained or transformed by milling: sub-Tg features and rejuvenation. *J Non Cryst Solids*. 2015;407:72–80. https://doi.org/10.1016/j.jnoncrysol.2014.08.055.
63. Khan KK, He YQ, Correia MA, Halpert JR. Differential oxidation of mifepristone by cytochromes P450 3A4 and 3A5: selective inactivation of P450 3A4. *Drug Metab Dispos*. 2002;30(9):985–990. https://doi.org/10.1124/dmd.30.9.985.
64. Iyer J, Saraf I, Ray A, Brunsteiner M, Paudel A. Assessment of diverse solid−state accelerated autoxidation methods for droperidol. *Pharmaceutics*. 2022;14(6):1–14. https://doi.org/10.3390/pharmaceutics14061114.
65. Trasi NS, Byrn SR. Mechanically induced amorphization of drugs: a study of the thermal behavior of cryomilled compounds. *AAPS PharmSciTech*. 2012;13(3):772–784. https://doi.org/10.1208/s12249-012-9801-8.
66. Trasi NS, Boerrigter SXM, Byrn SR. Investigation of the milling-induced thermal behavior of crystalline and amorphous griseofulvin. *Pharm Res*. 2010;27:1377–1389. https://doi.org/10.1007/s11095-010-0129-3.
67. Willart JF, Descamps M. Solid state amorphization of pharmaceuticals. *Mol Pharm*. 2008;5(6):905–920. https://doi.org/10.1021/mp800092t.
68. Descamps M, Willart JF. Perspectives on the amorphisation/milling relationship in pharmaceutical materials. *Adv Drug Deliv Rev*. 2016;100:51–66. https://doi.org/10.1016/j.addr.2016.01.011.
69. Hu Y, Macfhionnghaile P, Caron V, et al. Formation, physical stability, and quantification of process-induced disorder in cryomilled samples of a model polymorphic drug. *J Pharm Sci*. 2013;102(1):93–103. https://doi.org/10.1002/jps.23338.
70. Feng T, Pinal R, Carvajal MT. Process induced disorder in crystalline materials: differentiating defective crystals from the amorphous form of Griseofulvin. *J Pharm Sci*. 2008;97(8):3207. https://doi.org/10.1002/jps.
71. Brodka-Pfeiffer K, Häusler H, Graß P, Langguth P. Conditioning following powder micronization: influence on particle growth of salbutamol sulfate. *Drug Dev Ind Pharm*. 2003;29(10):1077–1084. https://doi.org/10.1081/DDC-120025865.
72. Lim RTY, Hoong AYJ, Ng WK, Tan RBH. Anomalous size evolution of partially amorphized pharmaceutical particles during post-milling storage. *Powder Technol*. 2015;286:1–8. https://doi.org/10.1016/j.powtec.2015.08.002.
73. *PubChem and Drugbank-Mifepristone*. 2022.. Accessed September 30; https://go.drugbank.com/drugs/DB00834.
74. Beckwith ALJ, Eichinger PH, Mooney BA, Prager RH. Amine autoxidation in aqueous solution. *Aust J Chem*. 1983;36(4):719–739. https://doi.org/10.1071/CH9830719.
75. Kajdas C. Mechanical activation of chemical process. *Mater Sci Appl*. 2015;06(01):60–67. https://doi.org/10.4236/msa.2015.61008.
76. Beyer MK, Clausen-Schaumann H. Mechanochemistry: the mechanical activation of covalent bonds. *Chem Rev*. 2005;105(8):2921–2948. https://doi.org/10.1021/cr030697h.
77. Zong Z, Qiu J, Tinmanee R, Kirsch LE. Kinetic model for solid-state degradation of gabapentin. *J Pharm Sci*. 2012;101(6):2123–2133. https://doi.org/10.1002/jps.23115.
78. Mehta M, Ragoonanan V, Mckenna GB, Suryanarayanan R. Correlation between molecular mobility and physical stability in pharmaceutical glasses. *Mol Pharm*. 2016. https://doi.org/10.1021/acs.molpharmaceut.5b00853.
79. Phan AD, Wakabayashi K. Theory of structural and secondary relaxation in amorphous drugs under compression. *Pharmaceutics*. 2020;12(2):1–11. https://doi.org/10.3390/pharmaceutics12020177.